ChemistrySelect

ChemistrySelect
Chemistry Europe
European Chemical Societies Publishing

RESEARCH ARTICLE OPEN ACCESS

TXCA-Mediated Synthesis of Halogenated 4-Aminocoumarins Derivatives Under Mild Conditions and In Silico Evaluation Against Alzheimer's Disease-Related Protein Targets

Maryelle A. G. de Carvalho[1] | Vinicius C. Alves[1] | Lara M. Flores[1] | Carlos V. Doerner[1] | Tácia K. Hall[2] | Cristiani F. Bortolatto[2] | Louis P. Sandjo[1] | José S. S. Neto[3] | Antonio L. Braga[1] | Francisco F. de Assis[1]

[1]Departament of Chemistry, CFM, Universidade Federal de Santa Catarina, Florianópolis, Santa Catarina, Brazil | [2]Laboratory of Biochemistry and Molecular Neuropharmacology (LABIONEM), Graduate Program in Biochemistry and Bioprospecting (PPGBIO), Chemical Pharmaceutical and Food Sciences Center (CCQFA), Universidade Federal de Pelotas, Pelotas, Rio Grande do Sul, Brazil | [3]Laboratory of Sustainable Organic Synthesis and Technologies (SustenSin), Institute of Chemistry, Universidade Federal de Goiás, Goiânia, Goiás, Brazil

Correspondence: José S. S. Neto (zeneto.qmc@gmail.com) | Antonio L. Braga (braga.antonio@ufsc.br) | Francisco F. de Assis (assis.francisco@ufsc.br)

Received: 1 November 2025 | **Revised:** 6 April 2026 | **Accepted:** 6 April 2026

Keywords: Alzheimer's disease| aminocoumarins| halogenation| in silico| neuroprotection| trihaloisocyanuric acids

ABSTRACT

A highly efficient and selective protocol for the halogenation of the C—H bond of 4-aminocoumarin derivatives is reported. This shows that the use of trihaloisocyanuric acids in the synthesis of aminocoumarin derivatives consists of obtaining pharmacologically important compounds using new strategies and transformations. The proposed method has a broad substrate scope and uses ethyl acetate as the solvent. The reaction scope evaluation of 4-aminocoumarins with different structural characteristics showed that the reaction tolerates electron-withdrawing groups (compounds **3d–f** and **8c–e**) and electron-donating groups (compounds **3b-c**, **3g**, **5**, **7**, and **8b**). A sterically hindered group attached to the nitrogen at C4 was also tolerated in the bromination reaction (compound **3h**), as well as an alkyl group (compound **7**) and even the absence of a substituent on the nitrogen (compound **5**). Molecular docking results show that, among the compounds tested, compound **3h** stands out. Its predicted interactions with acetylcholinesterase (AChE), monoamine oxidase B (MAO-B), β-secretase enzyme (BACE), and N-methyl-D-aspartate receptors (NMDAR) suggest a promising profile for inhibiting these neurochemical enzymes and antagonizing glutamatergic NMDAR, potentially contributing to therapeutic strategies for neurodegenerative diseases such as Alzheimer's disease.

1 | Introduction

Coumarins are naturally occurring secondary metabolites produced by microorganisms and plants [1]. These 2-H-chromen-2-one derivatives have rapidly become attractive due to their broad spectrum of biological activities, among additional applications [2–4]. Previous studies showed that coumarins possess antibacterial, antifungal, antiviral, antioxidant, anticancer, anticoagulant and anti-inflammatory activities, among others [5–11]. Thus, the coumarin scaffold has been of interest in drug discovery. 4-Aminocoumarins are a class of synthetic coumarin derivatives usually obtained from nucleophilic substitution reactions between amines and 4-hydroxycoumarins [8]. Members of this family have significantly shown diverse biological activities, especially anticancer [12–17] (Figure 1).

The presence of the amino group at position C-4 plays a pivotal role in the chemical reactivity of these compounds by

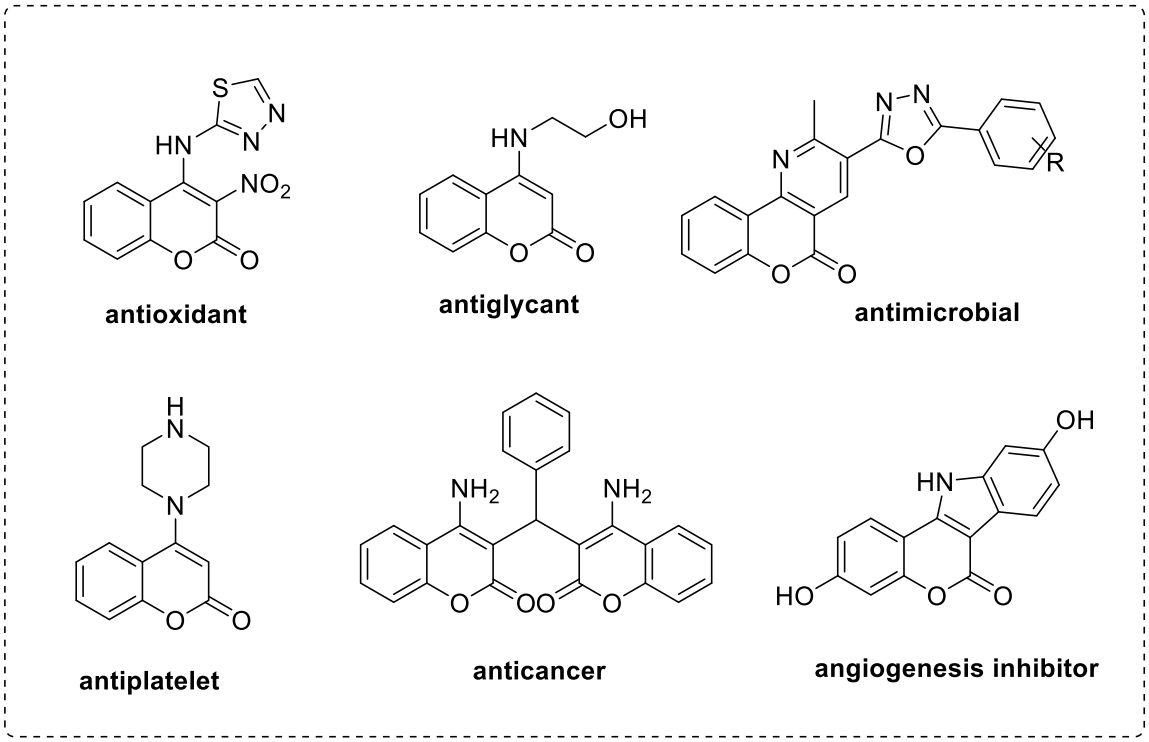

FIGURE 1 | Derivatives of aminocoumarins with biological activities.

enhancing the electronic density of C3 and subsequently its nucleophilicity. The reactivity of C3 has been explored in 4-aminocoumarins during synthetic reactions such as formylation, alkylation, arylation, selenylation, thiocyanation and others [8, 18–26]. These strategies have proven to be useful in the search for bioactive compounds derived from 4-aminocoumarins and highlight the relevance of pursuing the development of new synthetic methodologies that widen the possibility for structure diversification.

The halogenation of aromatic hydrocarbons and heterocycles represents a fundamental reaction in organic synthesis, significantly expanding the arsenal of methods available for constructing complex organic molecules [27]. This transformation not only enables the synthesis of highly valued intermediates but also produces organohalogen compounds that play essential roles in a wide range of applications [28, 29]. In particular, halogen incorporation into natural products can dramatically alter their physicochemical properties due to pronounced electronic and steric effects. These modifications arise from the distinct size and electronegativity of halogen atoms relative to hydrogen or other substituents, leading to changes in molecular polarity, lipophilicity, and overall reactivity. As a result, halogenated compounds often exhibit higher permeability across the blood-brain barrier, along with enhanced binding affinity and selectivity toward specific biological targets, which can significantly influence their pharmacological profiles by improving receptor interactions, increasing metabolic stability, and enhancing bioavailability [30–33] (Figure 2).

The pharmaceutical industry has particularly benefited from strategic halogenation, with approximately 25% of drugs and drug candidates containing at least one halogen atom [34]. This underscores the importance of halogenation in optimizing pharmacokinetic properties and enhancing therapeutic efficacy [35, 36]. Moreover, the formation of carbon-halogen (C—X) bonds is a crucial step in organic synthesis, serving as key intermediates in substitution and cross-coupling reactions [37]. Notably, palladium-catalyzed methodologies, such as Suzuki–Miyaura and Heck cross-coupling reactions, have revolutionized the pharmaceutical industry by enabling the efficient synthesis of bioactive molecules, including anticancer and antiviral drugs [38].

Beyond pharmaceuticals, halogenated compounds play a vital role in agrochemical and advanced materials, where halogens help define key physicochemical properties that influence stability, bioavailability, and biological interactions. Strategic halogenation thus remains a powerful tool in medicinal chemistry and beyond, enabling the fine-tuning of molecular interactions and the optimization of lead compounds for diverse applications [39, 40].

Traditionally, the introduction of halogen atoms in organic frameworks consists of electrophilic substitution in aromatic and heteroaromatic compounds with electrophilic halogen species [41]. Classical electrophilic aromatic halogenation using X_2 is still a useful synthetic tool, but the difficulties associated with the manipulation of molecular halogens and the lack of chemoselectivity narrow down its use. To avoid the use of excess molecular halogens (mainly Cl_2 and Br_2) and strong chemical oxidizers, other environmentally friendly halogenation methods have been developed in recent decades [42–44].

Trichloroisocyanuric acid (TCCA) is a widely used chlorinating agent, renowned not only for its effectiveness as a bleach and

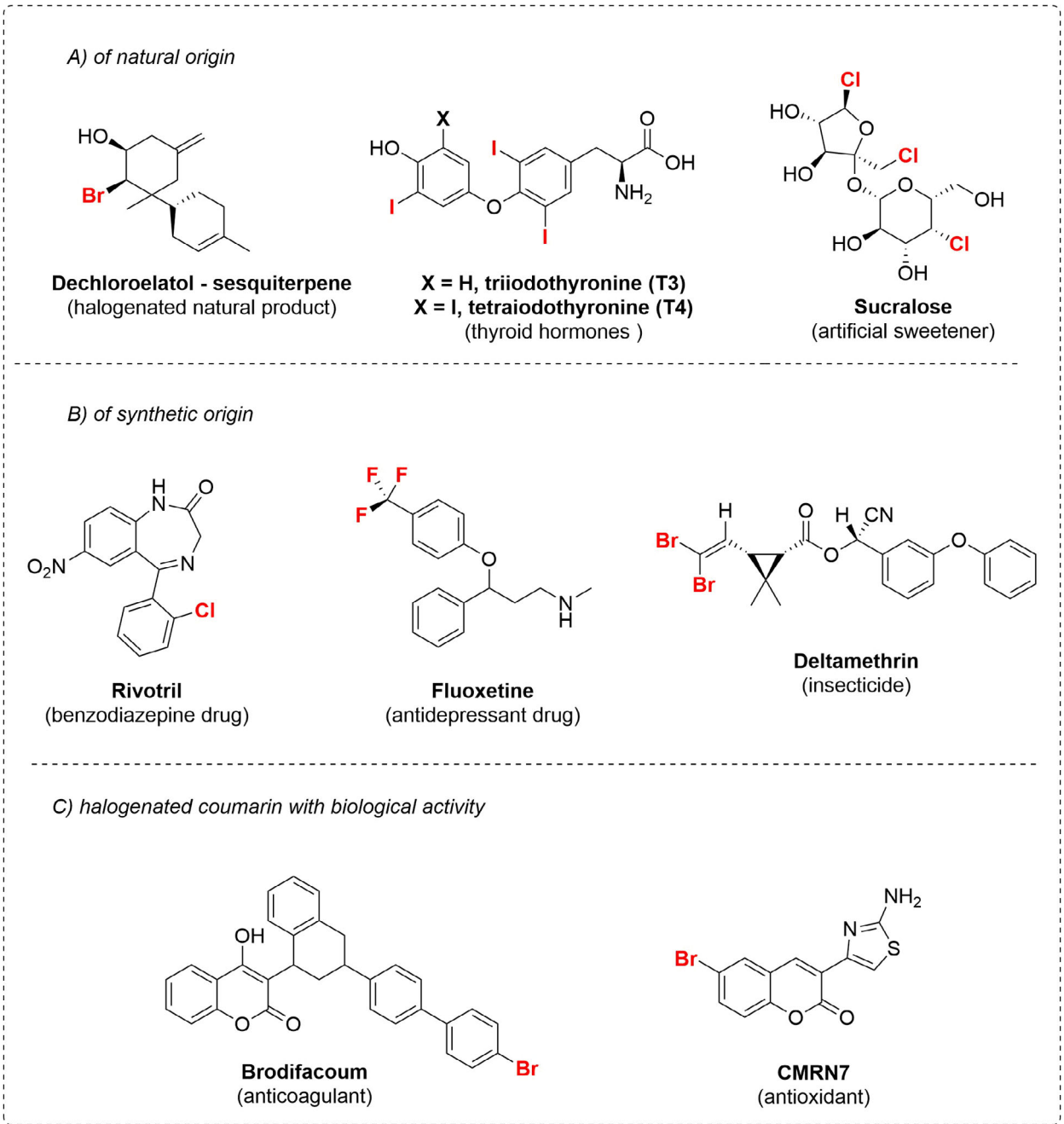

FIGURE 2 | Examples of halogenated compounds: (A) Natural origin; (B) Synthetic origin; (C) Halogenated coumarin with biological activity.

its bactericidal properties but also for its low cost, remarkable stability, ease of handling, and ready accessibility [45, 46] (Scheme 1A).

These attributes make TCCA a green source of chlorine, and all trihaloisocyanuric acids (TXCAs, where X = Cl, Br, or I) have emerged as valuable halogenating agents for organic compounds. For instance, both TCCA and its bromine analog (TBCA) exhibit excellent atomic efficiency by generating up to three equivalents of the respective halogen in situ. This capability translates into effective reagent savings (up to a factor of 229), while promoting more sustainable and environmentally friendly halogenation processes [47–49]. Consequently, these reagents are ideal not only for laboratory-scale syntheses but also hold significant promise for large-scale industrial applications, aligning closely with modern green chemistry initiatives [50] (Scheme 1B).

To the best of our knowledge, literature contains only isolated reports on the halogenation of 4-aminocoumarins. A comprehensive and systematic study on the halogenation of these compounds would be useful for the design of new synthetic strategies toward the synthesis of novel bioactive 4-aminocoumarin derivatives. In this context, this study describes the development of a new, efficient, and rapid synthesis protocol for the direct halogenation of the C(sp^2)—H bond of 4-aminocoumarin derivatives using trihaloisocyanuric acids (TXCA, X = Cl and Br), providing a more sustainable protocol. In addition, molecular docking and absorption, distribution, metabolism, excretion, and toxicity

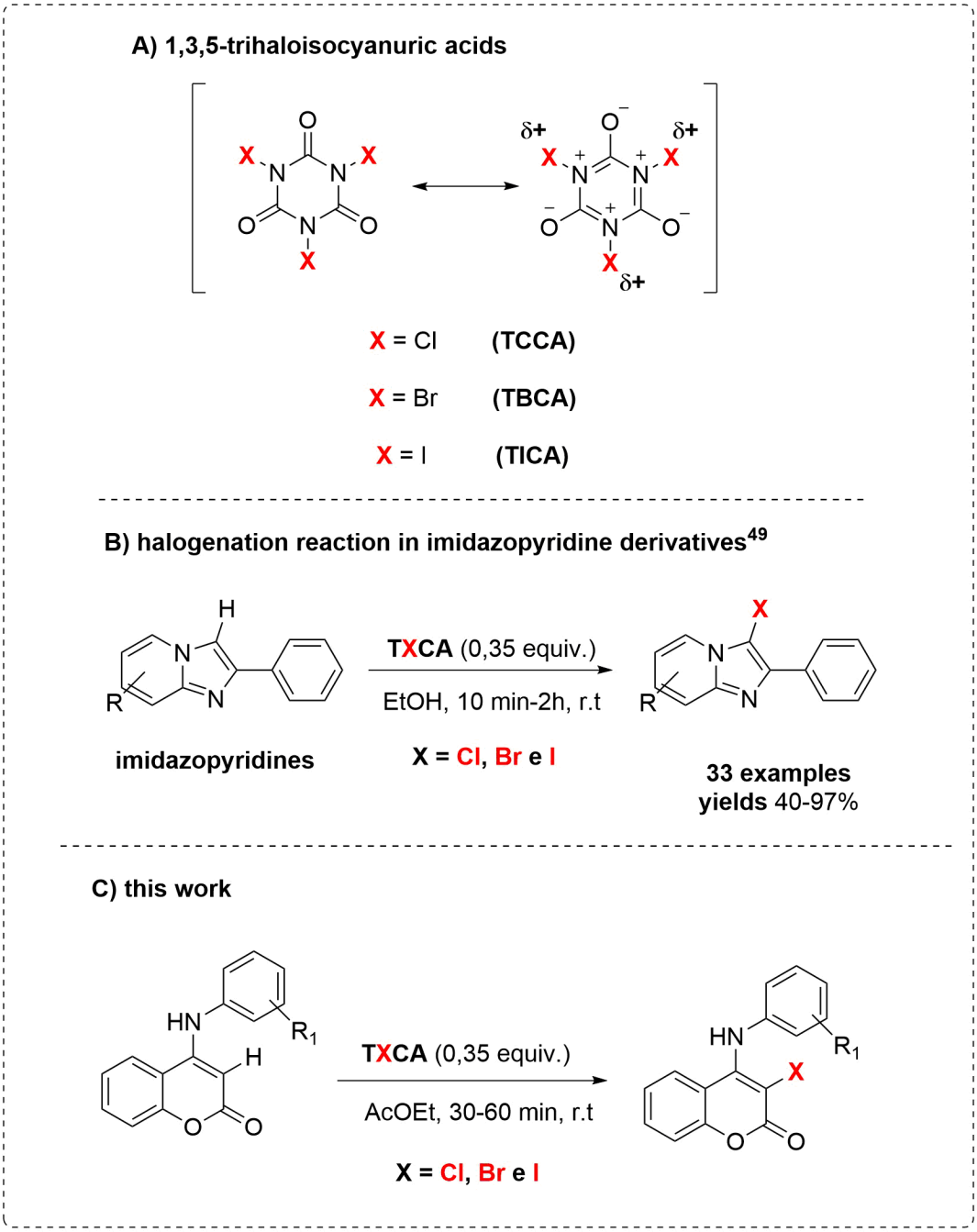

SCHEME 1 | (A) Types of 1,3,5-trihaloisocyanuric acids; (B) Halogenation reaction in imidazopyridine derivatives [50]; (C) This work.

(ADMET) profiling studies were performed with the halogenated coumarin derivatives obtained, to evaluate their interactions with biological targets related to Alzheimer's disease, since other similar structures have been identified as multitarget enzyme inhibitors related to neurodegenerative diseases [51]. Inhibiting specific enzymes and receptors in the central nervous system (CNS), such as acetylcholinesterase (AChE), monoamine oxidase B (MAO-B), and beta-secretase enzymes (BACE), or N-methyl-D-aspartate receptors (NMDAR), offers promising therapeutic approaches for AD [52].

2 | Results and Discussion

Initially, the optimization process to determine the optimal reaction conditions began by selecting tribromoisocyanuric acid (TBCA) as the halogenation agent. This choice was made due to the intermediate reactivity of bromine compared to chlorine and iodine. Consequently, we anticipated that the reaction conditions established during the optimization process would be more likely to yield good results with both TCCA and TICA (triiodoisocyanuric acid).

TABLE 1 | Optimization study of the reaction conditions for the synthesis of product **3a**.[a]

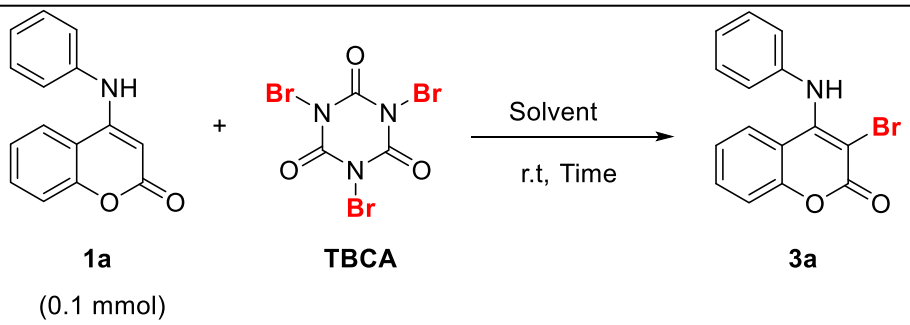

1a (0.1 mmol) **TBCA** **3a**

Entry	TBCA (equiv.)	Solvent	Temperature (°C)	Time (min.)	Yield of 3a (%)[b]
1	0.35	EtOH	r.t	120	73
2	0.17	EtOH	r.t	120	15
3	0.50	EtOH	r.t	120	13
4	1.0	EtOH	r.t	120	15
5	0.35	MeOH	r.t	120	14
6	0.35	DCM	r.t	120	13
7	0.35	MeCN	r.t	120	41
8	0.35	Acetone	r.t	120	85
9	0.35	H_2O	r.t	120	Trace
10	0.35	Acetone/H_2O (3:1)	r.t	120	58
11	0.35	AcOEt	r.t	120	88
12	0.35	AcOEt	r.t	60	64
13	0.35	AcOEt	r.t	90	86
14	0.35	AcOEt	r.t	150	96
15[c]	0.35	AcOEt	r.t	150	90
16[c]	0.35	AcOEt	r.t	60	90
17[c]	**0.35**	**AcOEt**	**r.t**	**30**	**85**
18[c]	0.35	AcOEt	r.t	15	70
19[c]	0.35	AcOEt	50	15	60

[a]Reaction carried out under atmosphere conditions with 2 mL of solvent (0.05 mol.L^{-1} in relation to **1a**).
[b]Isolated yield.
[c]Reaction carried out with 1 mL of solvent (0.1 mol.L^{-1} in relation to **1a**).

The 4-(phenylamino)coumarin **1a** was chosen as the model substrate for the bromination reaction. We began our study by using 0.1 mmol of **1a**, 0.35 equiv. of TBCA in ethanol as a solvent. After 2 h at room temperature, total consumption of substrate **1a** was observed, and brominated aminocoumarin **3a** was obtained in 73% yield after column chromatography purification (Table 1, entry 1). Furthermore, we decided to vary the amount of TBCA to check if this could improve the yield of product **3a**. The bromination reaction proved to be dependent on the amount of TBCA equivalents, where the use of 0.17, 0.5, and 1.0 equiv. led to the formation of the reaction product **3a** with yields of 13% to 15% (Table 1, entries 2–4). The ideal amount of TBCA was therefore set at 0.35 equiv. (Table 1, entry 1). Next, the reaction was carried out by replacing ethanol with other solvents. The use of solvents such as methanol, dichloromethane, acetonitrile, and acetone afforded compound **3a** with yields ranging 13% to 85% (Table 1, entries 5–8). When water was used, only trace amounts of product **3a** were detected, and a mixture of acetone/water 3:1 provided 58% yield for the target compound (Table 1, entries 9-10). The use of AcOEt as a solvent was able to provide the reaction product with 88% yield (Table 1, entry 11), therefore, it was chosen as the reaction solvent.

It was also assessed whether the reaction time would influence the yield of the halogenation product **3a**. Reducing the reaction time to 60 min led to a decrease in yield to 64% (Table 1, entry 12). When the reaction was conducted for 90 min, there was no significant change in the yield of **3a**, while increasing the reaction time to 150 min led to the formation of the desired product in 96% yield (Table 1, entries 13 and 14).

Adopting 150 min as the best time to carry out the reaction, we moved on to the last reaction parameter to be evaluated, which was concentration. Increasing the concentration of the reaction medium to 0.1 mol.L^{-1} (in relation to **1a**) allowed product **3a** to be obtained still in a very satisfactory yield of 90% (Table 1, entry 15).

We wondered whether it would be possible to reduce the reaction time at this new concentration without significant losses in yield. When the reaction was carried out at a concentration of 0.1 mol.L^{-1} for periods of 30 and 60 min, product **3a** was formed in yields of 85%–90% (Table 1, entries 16 and 17). These results show that there is no significant loss of efficiency when reaction time is reduced to 30 min. On the other hand, when the reaction was performed 15 min the yield of **3a** was significantly lower (70%) (Table 1, entry 18). Although 70% is still a good yield, we believe that it is more advantageous to keep the reaction going for 30 min and achieve a yield of 85%. Lastly, we evaluated if heating could increase the yield of compound **3a** in the 15-min condition, but the effect produced was the opposite and a yield of 60% was obtained when the reaction was carried out at 50 °C for 15 min (Table 1, entry 19). At the end of this study, we concluded that the best condition for obtaining **3a** is that described in entry 17 of Table 1, using 0.35 equiv. of TBCA, AcOEt as the solvent, room temperature, a concentration of 0.1 mol.L^{-1} and a reaction time of 30 min.

With the optimum reaction conditions for the formation of 3-bromo-4-(phenylamino)coumarin **3a** in hand, we moved toward the evaluation of the substrate scope of the methodology. First, we investigated the reaction behavior when derivatives of compound **1a** were used. Eight examples were obtained from these studies, which provided the products of interest **3a–h** with yields ranging from 42% to 98% (Scheme 2).

We evaluated the influence of substituents in position 4 of the aromatic ring. Substrates bearing electron-donating and electron-withdrawing groups were used and the corresponding products **3a–f** were obtained in good to excellent yields. It is worth noting that an additional 30 min were required to obtain products **3b** and **3g**. The reaction using the bulky naphthyl substrate gave two products, with **3h** as the major one, obtained in 55% yield, and the other in trace amount.

The methodology described was also explored using coumarins **4** and **6**, containing the NH_2 group and the benzyl group, respectively (Scheme 3). As with the 4-*(N-a*rylamino)coumarins, the novel bromination product was obtained in good yield (77%), demonstrating that the presence of the aliphatic group, as well as the absence of a substituent at the nitrogen was well tolerated, with good reaction behavior.

We also evaluated the scalability of the reaction by carrying out an experiment on a gram scale. First, we carried out the reaction at 0.5 mmol of compound **1a**, at a concentration of 0.1 M for 75 min and, to our delight, the target product generated 66% yield. When the reaction was performed with 1.5 mmol of **1a**, it took 24 h, affording the product with a yield of 24%. We decided to repeat the reaction and reduce the reaction time to 5 h, obtaining a product yield of 69%.

To further evaluate the scalability, we increased the reaction scale to 4.5 mmol of coumarin **1a** (Scheme 4). It is worth noting that this reaction proved to be faster than the others, taking only 120 min for the starting material to be consumed. In this condition, the brominated coumarin **3a** was isolated in 54% yield. For all the scale-up experiments, the consumption of the starting material took longer compared to the small-scale reaction, which is not uncommon due to changes in energy and mass transfer phenomena.

Based on the results achieved with TBCA, we decided to see if the optimum reaction condition found for the bromination of coumarins **1** could lead to the chlorination product when used with TCCA. To our satisfaction, compound **1a** was converted into the corresponding chlorinated product **8a** with a 43% yield (Scheme 5). Based on this result, we used some of the previously described substrates to evaluate the scope of the reaction with TCCA. From this study we obtained 5 examples (**8a–e**) which provided products of interest with yields ranging from 43% to 82%.

We evaluated the performance of the reaction by varying the in substrate. The presence of an electron-withdrawing group on the aromatic ring provided the corresponding product (**8c–e**) above 60%. For the substrate with an electron-donating group (**8b**), the desired product was obtained in moderate yield, and no additional time was required. Finally, it can be said that the optimum condition previously established for the reaction involving TBCA also proved to be effective for the formation of the chlorinated products obtained using TCCA.

Reactions with TICA were also carried out under the same conditions used for bromination and chlorination of 4-aminocoumarins **1**. Substrates **1b**, **1d**, and **1e** were subjected to the reaction with TICA, but only **1b** and **1d** were able to afford the corresponding iodinated products **10a** and **10b**, albeit in a low yield of 16%-21%(Scheme 6). Attempts to improve the yield of the iodination products were made, including treatment of the silica gel to avoid degradation during purification, addition of a base to the reaction medium, use of excess of TICA, and change of solvent, among others (see Supporting Information—SI for more details). Afterwards, we found a slight improvement in the yield of compound **10b**, which was obtained in 33% yield.

According to the results obtained, iodination with TICA proved to be much less efficient than bromination with TBCA or chlorination with TICA. Although some conditions were able to provide iodinated products, we noticed low reproducibility in these experiments, which compromises the viability of this approach as a way of obtaining iodinated 4-aminocoumarins. Given this, we decided not to continue with the studies involving TICA and 4-aminocoumarins.

2.1 | Mechanistic Studies

Once the studies to determine the reaction scope for the methodology were completed, we proceeded to carry out planned experiments with the aim of the mechanism by which the reaction occurs.

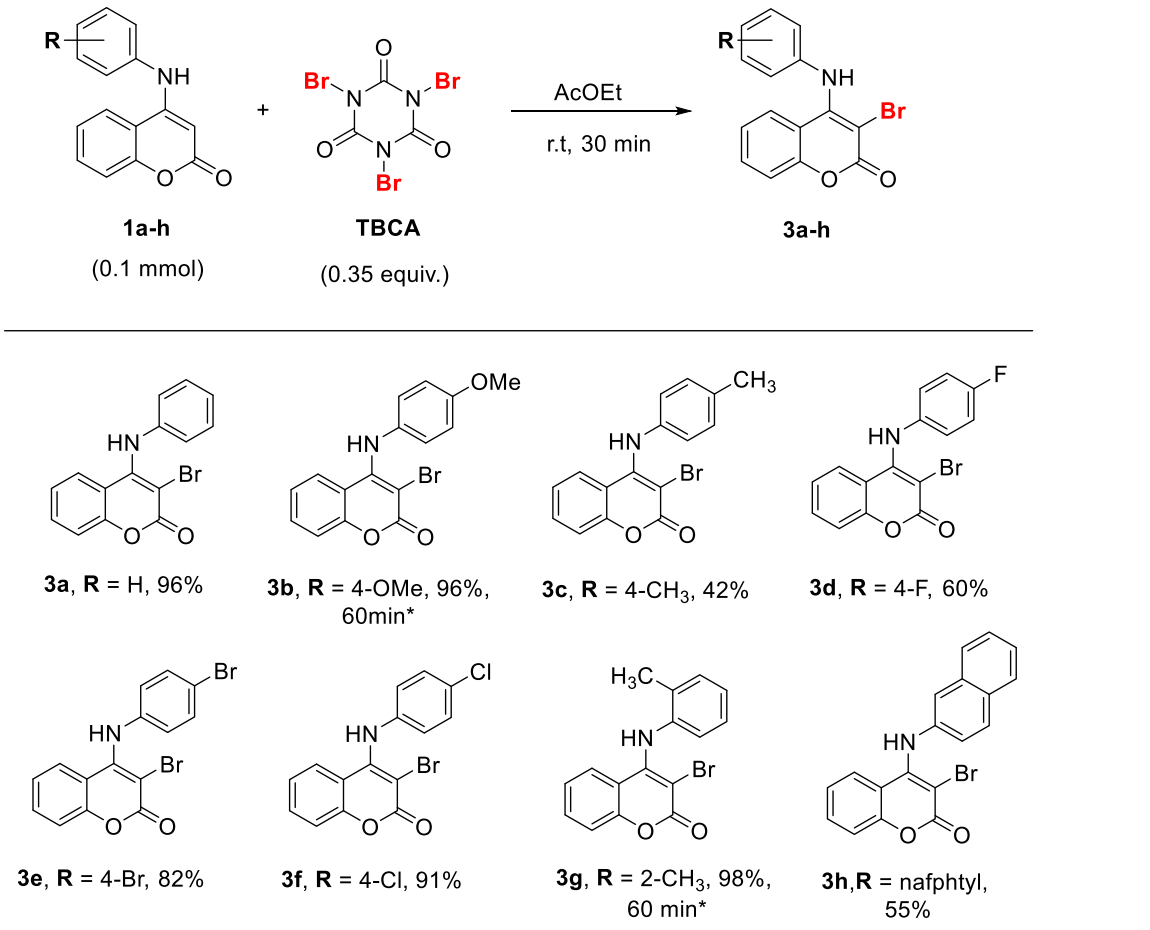

SCHEME 2 | Reaction between coumarins **1a–h** and TBCA.

2.2 | Modified Reaction Atmosphere Studies

Two studies were carried out using modified atmospheres. First, the reaction was carried out maintaining the reaction parameters already established, but with a pure O_2 reaction atmosphere. This experiment aimed to investigate whether the process follows a radical reaction mechanism. Molecular oxygen is a biradical species, characterized by having two unpaired electrons in its frontier orbitals. Thus, the presence of radicals in the reaction could lead to their rapid reaction with the molecular oxygen present in the medium, which could interrupt the progress of the reaction. Therefore, if this occurred, a significant reduction in the reaction yield would be expected. However, the yield observed in this experiment was 92% (Scheme 7A), which is similar to that observed without changing the reaction atmosphere. This result indicates that the reaction mechanism may not involve radical species. In the second study, the reaction was carried out in an argon atmosphere, to check whether the oxygen or water present in the atmospheric air had any effect on the reaction. However, the yield observed in this study was also 92%. It can therefore be concluded that none of the components of atmospheric air play any role in the reaction mechanism.

2.3 | Reaction in the Presence of a Radical Inhibitor

Some experiments were carried out to help us understand the reaction mechanism. The first experiments carried out involved the use of radical inhibitors such as 2,2,6,6-tetramethyl-piperidi-1-nyl)oxyl (TEMPO) and 2,6-di-*tert*-butyl-4-methylphenol (BHT) (Scheme 7B). In the experiment with TEMPO, product **3a** was obtained in 46% yield, *i.e.*, approximately half the yield obtained when the radical inhibitor was not present (85%). However, in the experiment with BHT, the yield obtained for the brominated product was close to the reference value. These results do not lead us to a clear conclusion about the possible involvement of a radical mechanism, although the result obtained with TEMPO is a good indication.

2.4 | Mechanism Proposal

Based on the experiments previously discussed and the reports in the literature [50, 53, 54], we believe there might be an ionic path and a radical path operating in parallel for the bromination of 4-aminocoumarins using TBCA (Scheme 8).

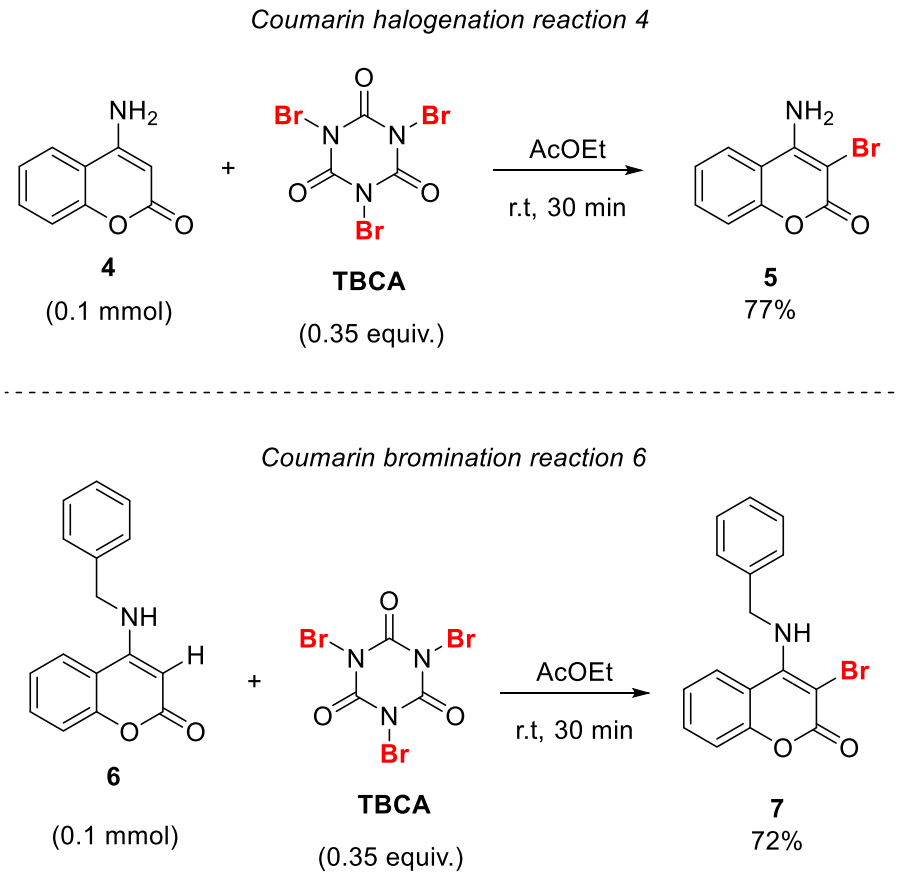

SCHEME 3 | Reaction using coumarins **4** and **6**.

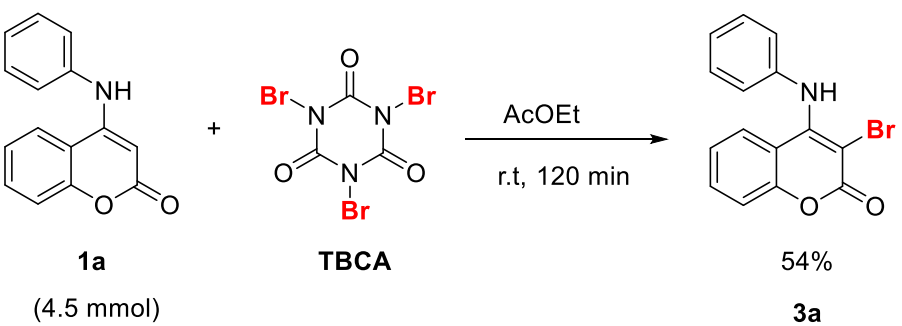

SCHEME 4 | Scale-up reaction for the bromination coumarin **1a**.

For the Ionic path (Scheme 8a), we expect the first step should be the nucleophilic attack of **1** to one of the bromine atoms of TBCA. This step should be facilitated by the labile nature of the N—Br bond and the stability of the carbocation placed next to both the aromatic ring and the nitrogen atom in intermediate **II**. Next, proton abstraction from intermediate **II**, mediated by the anion **I**, would restore the α,β-unsaturated double bond, affording debrominated TBCA **III** and the corresponding halogenated product **3**. In the alternative radical path (Scheme 8b), initiation should occur through homolytic cleavage of the N—Br bond in TBCA, affording the bromine radical (Br•) and the nitrogen radical **IV**. The addition of Br• to coumarin **1** should form radical **V**, which should benefit from the same structural features mentioned in the case of carbocation **II**, as both are electron-deficient carbon species. In the final step, hydrogen atom abstraction (HAT) from **V** should afford **III'**, which is essentially the same as **III**, as both are tautomers, along with corresponding halogenated product **3**.

2.5 | Molecular Docking

A virtual screening was carried out with all compounds using molecular docking tools. As summarized in Table 2, the tested compounds exhibited similar binding affinities with the protein targets (AChE, BACE, MAO-B, and NMDAR). Among them, com-

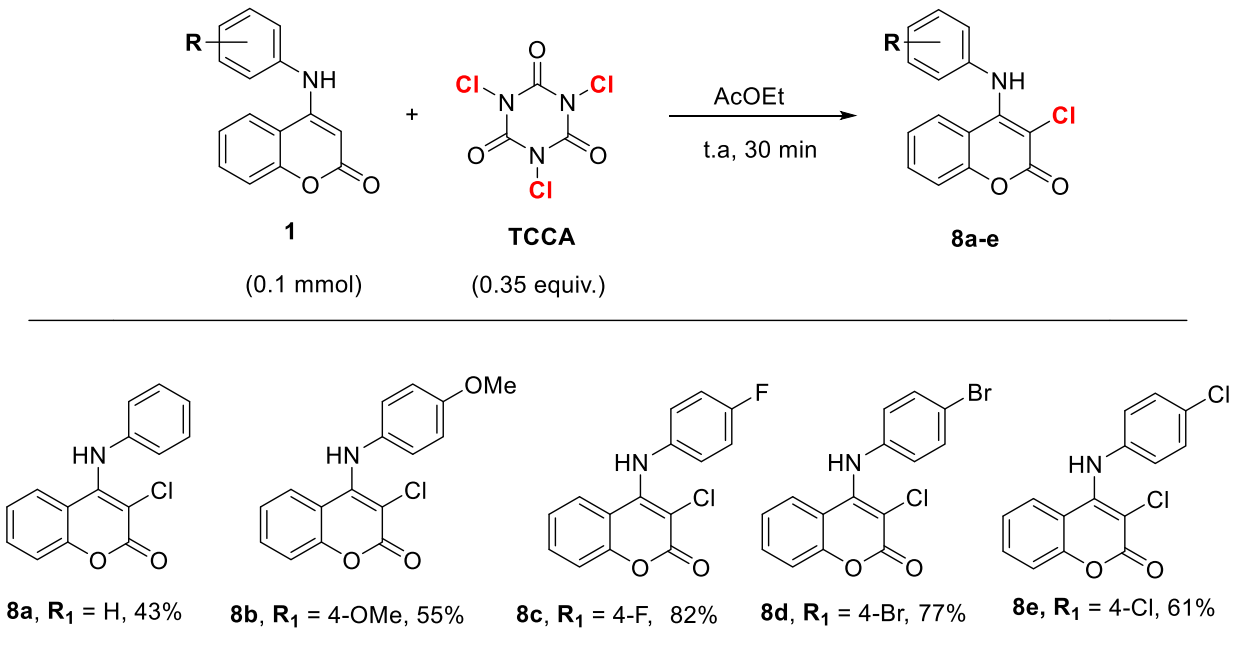

SCHEME 5 | Evaluation study of the chlorination reaction scope of compounds **1** with TCCA.

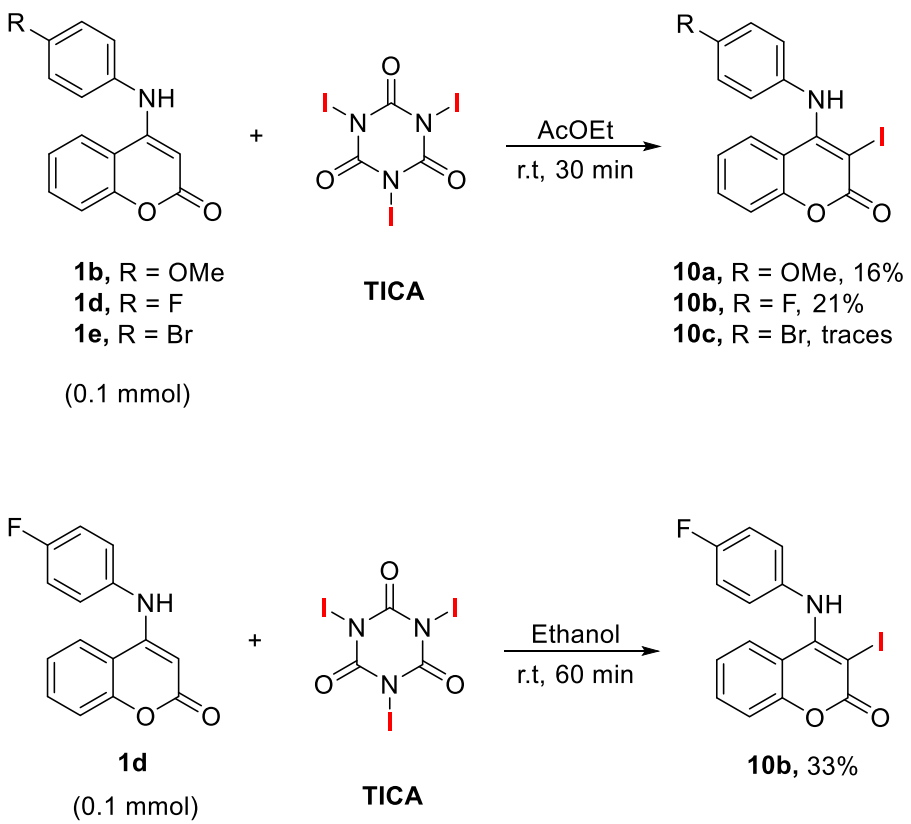

SCHEME 6 | Iodination of 4-aminocoumarins **1b**, **1d**, and **1e** using TICA.

pound **3h** has reached the lowest docking scores (stronger binding affinity). Their docking scores were lower than those demonstrated for drug prototypes or medicines (positive controls). Thus, compound **3h** demonstrated superior in silico potential for interacting with different protein targets associated with AD.

AChE is a crucial enzyme in the degradation of acetylcholine (ACh) in the CNS. Reduced ACh levels are implicated in the pathophysiology of cognitive dysfunction occurring in AD. Therefore, enhancing cholinergic neurotransmission by AChE inhibitors (*e.g.* rivastigmine) has been established as an AD

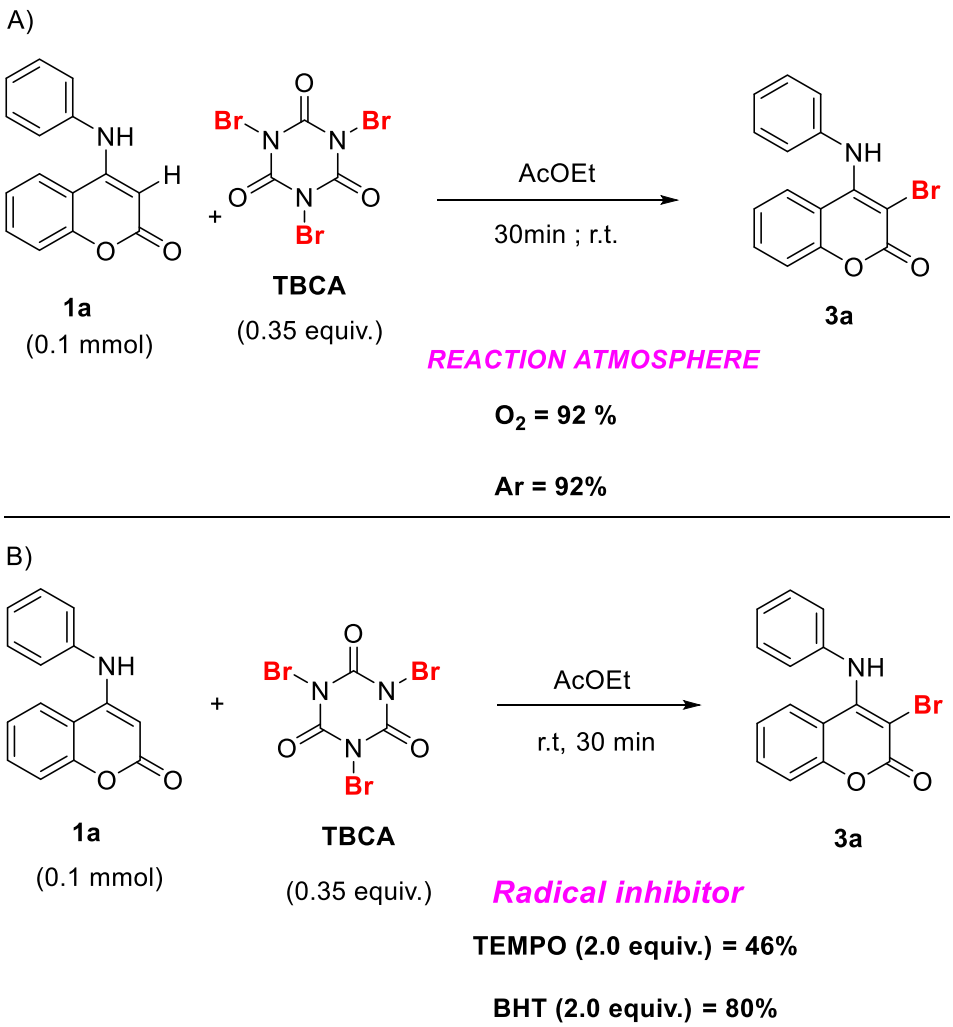

SCHEME 7 | Mechanistic studies with (A) modified reaction atmosphere, and (B) presence of radical inhibitors.

therapeutic strategy [55]. We demonstrated that all tested compounds exhibited low binding energies (less than -9 kcal/mol) for human AChE, with a particular emphasis on compounds **3h** (-10.3 kcal/mol), followed by **3c** and **8e** (−9.9 kcal/mol), which outperformed the positive control, rivastigmine (−7.3 kcal/mol). Studies indicate that residues such as Trp286 and Phe338 are essential for substrate binding and the stability of the enzyme-inhibitor complex [56, 57]. Docking results showed that our compounds interact with these critical residues, suggesting that their inhibitory potency may result from effectively blocking substrate access to the catalytic site, as evidenced by the low binding energies, especially for compound **3h**.

Compound **3h** was selected for an in-depth presentation of interaction diagrams (Figures 3–6). We also selected three other compounds with high target binding affinities (**3c**, **3g**, and **8e**) based on the best docking scores for at least two targets and included their interaction diagrams in the Supplementary Material (Figure S1–S12).

As shown in Figure 3A, compound **3h** interacted with AChE through multiple molecular interactions. The amino acid residues Trp86, Gly121, Phe338, Phe297, Phe295, Val294, Tyr341, Asp74, Asn87, and Tyr72 were involved in Van der Waals interactions. Moreover, Ser125 and Tyr124 contributed to Pi-donor hydrogen bonds. Pi-Pi stacking and Pi-Pi T-shaped interactions were observed with Trp286.

Another tested target, MAO-B, plays a crucial role in the degradation of monoaminergic neurotransmitters. MAO inhibitors such as selegiline have been applied to mitigate symptoms of AD. Furthermore, as MAO enzymes are generators of reactive species, MAO- inhibition B can mitigate oxidative stress, a key factor involved in neurodegeneration. In this study, compounds **3c, 3g, 3h** (−11.4 kcal/mol), among others, exhibited significantly lower binding energies than selegiline (−7.3 kcal/mol). The compounds bind to the active site of the human MAO-B enzyme and interact with important residues. Trp388 plays a role in noncovalent binding to FAD, while Tyr398 and Tyr435 form an aromatic arrangement that stabilizes substrate binding [58, 59].

In its interaction with human MAO-B, compound **3h** exhibited several distinct molecular interactions. The amino acid residues Val294, Phe343, Arg42, Gln206, Tyr60, Ser59, Gly58, Cys172, Tyr326, Met436, and Gly434 were involved in Van der Waals interactions. Additionally, Pi-Pi interactions were observed with

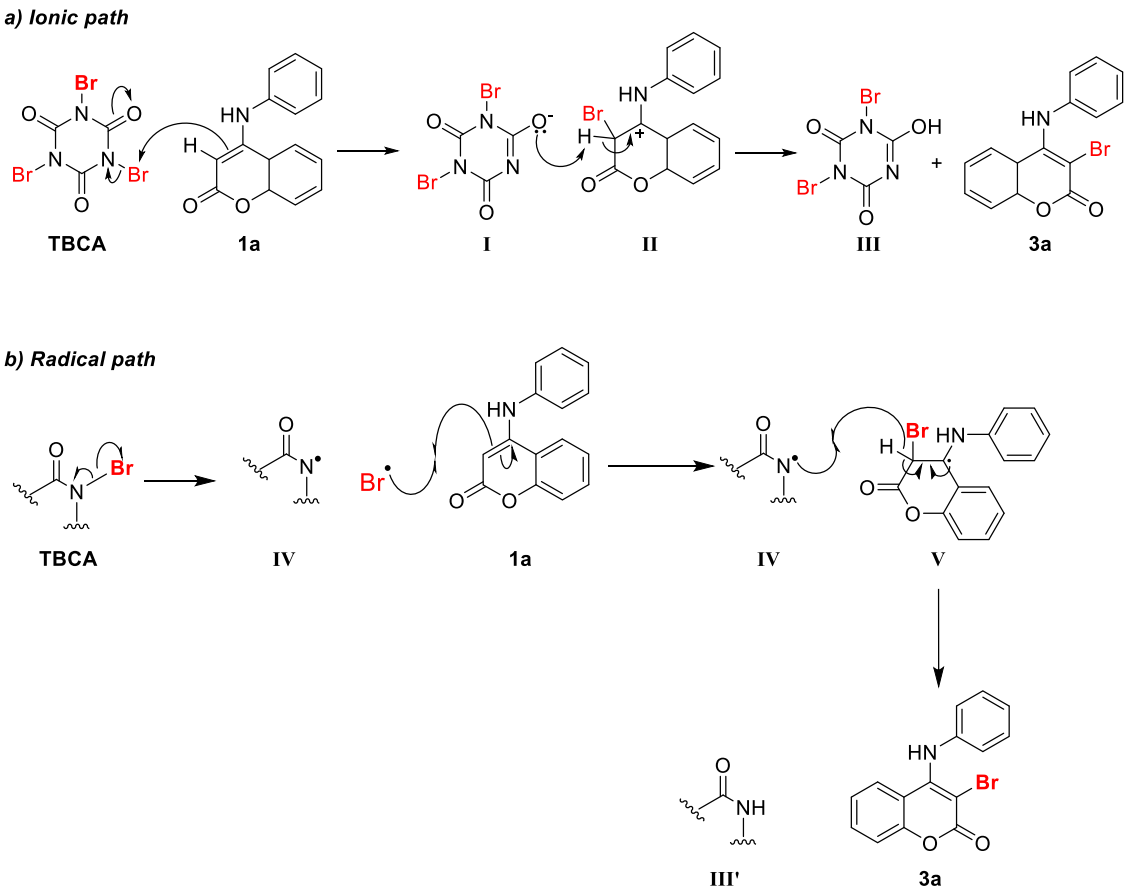

SCHEME 8 | Proposed mechanism for the bromination of 4-aminocoumarins with TBCA.

Trp388, Gly57, and Tyr398 residues. A conventional hydrogen bond was established with Cys397, while Lys296 and Leu171 participated in Pi-alkyl interactions (Figure 4A). These interactions with MAO-B are similar to those of selegiline, suggesting that compound **3h** exhibits an interaction profile comparable to that of the positive control.

Small-molecule inhibitors of BACE1 reduce Aβ peptide production and are leading drug candidates for AD. Although drugs such as verubecestat have been clinically tested, they were discontinued due to low efficacy or adverse effects [60]. Here, our in silico predictions indicate that different compounds, with an emphasis on **3h** (−9.3 kcal/mol) and **8e** (−8.2 kcal/mol, similar to verubecestat score), could have the potential to act as BACE1 inhibitors and interact with other targets. For BACE, residue Tyr71 plays a significant role in stabilizing the inhibitor's binding, contributing to a more durable and effective interaction at the enzyme's active site. Additionally, residues Ile126 and Arg128 are essential for interaction, suggesting these residues are critical for the initial binding and maintenance of the enzyme-inhibitor complex [61].

In Figure 5A, it can be observed that compound **3h**, upon interacting with BACE, displayed several molecular interactions. The amino acid residues Ile126, Ser36, Ser35, Asn37, Lys75, Lys107, and Phe108 were involved in Van der Waals interactions. Additionally, Ile118, Arg128, and Tyr71 formed Pi interactions, while Val69 mediated a Pi-sigma interaction, and Trp76 established a Pi-donor hydrogen bond.

Regarding NMDA receptor inhibition, studies have shown that modulating critical residues like Arg367 and Gly390 can significantly influence receptor function. Interactions with these residues can affect the receptor's role in synaptic plasticity, learning, and memory, which are essential processes in the CNS [62, 63]. Here, compounds **3g** (−8.0 kcal/mol) and **3h** (−8.1 kcal/mol) demonstrate a greater potential for interacting with this receptor compared with memantine (−5.3 kcal/mol), which is a reference glutamatergic drug for AD. Notably, the strong binding of **3g** and **3h** to residues Arg367 and Gly390 suggests that these compounds may effectively disrupt the receptor's interaction with its natural ligands, potentially altering its role in synaptic processes. This could enhance their efficacy as NMDA receptor inhibitors, thereby offering a promising approach for modulating receptor activity in AD.

Compound **3h**, upon interacting with NMDAR, involved amino acid residues Ala370, Lys368, and Phe369 in the formation of Pi-donor hydrogen bonds, while residues Arg367, Lys179, Pro142, Tyr372, Phe388, Gly390, Glu153, and Ser391 participated in Van der Waals interactions. Furthermore, while Leu149 mediated a Pi-sigma and Pi-alkyl interaction and Lys368 also established Pi-alkyl interaction, residues His146 and Asn362 also formed conventional hydrogen bonds (Figure 6A).

TABLE 2 | Molecular docking scores (Kcal/mol) of compounds **3a–h**, **5**, **7**, **8a–e**, **10a** and **10b** in relation to AChE, MAO-B, BACE, NMDAR.

Compounds	Docking scores (Kcal/mol)			
	AChE	BACE	MAO-B	NMDAR
3a	−9.2	−7.5	−9.7	−7.7
3b	−9.2	−7.9	−9.6	−7.6
3c	−9.9	−8.1	−10.2	−7.9
3d	−9.7	−7.9	−9.9	−7.9
3e	−9.7	−8.1	−10.1	−7.7
3f	−9.8	−8.0	−10.0	−7.8
3g	−9.3	−8.0	−10.2	−8.0
3h	−10.3	−9.3	−11.4	−8.1
5	−7.5	−6.3	−7.3	−5.8
7	−9.6	−8.1	−9.5	−7.4
8a	−9.3	−7.7	−9.7	−7.8
8b	−9.2	−7.9	−9.8	−7.5
8c	−9.8	−8.1	−9.9	−7.9
8d	−9.8	−8.2	−10.1	−7.6
8e	−9.9	−8.2	−9.9	−7.7
10a	−9.0	−7.7	−9.4	−7.6
10b	−9.5	−7.4	−9.6	−7.7
Rivastigmine (PC)	−7.3	—	—	—
Verubecestat (PC)	—	−8.2	—	—
Selegiline (PC)	—	—	−7.3	—
Memantine (PC)	—	—	—	−5.3

Abbreviations: AChE, Acetylcholinesterase; BACE, beta-secretase enzyme; MAO-B, monoamine oxidase B; NMDAR, N-methyl-D-aspartate receptor; PC, positive control.

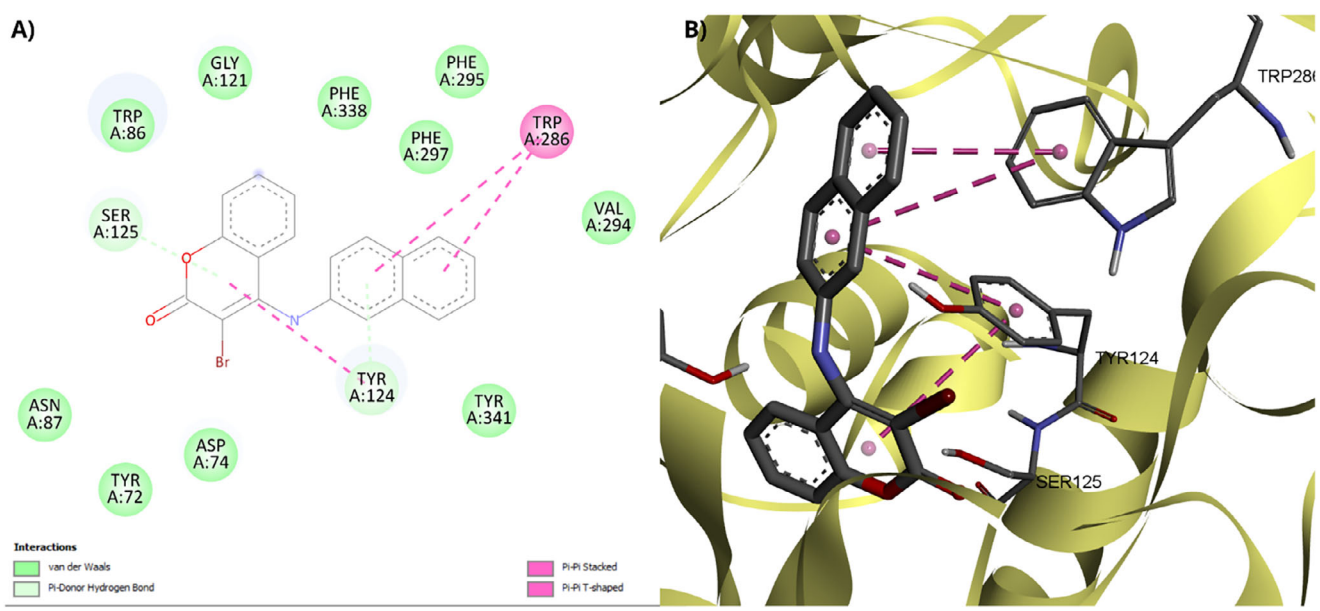

FIGURE 3 | The molecular docking results of compound **3h** are depicted by (A) protein-ligand interactions with the human AChE enzyme in 2D format and (B) ligand-enzyme interactions in 3D format (PDB ID: 4PQE).

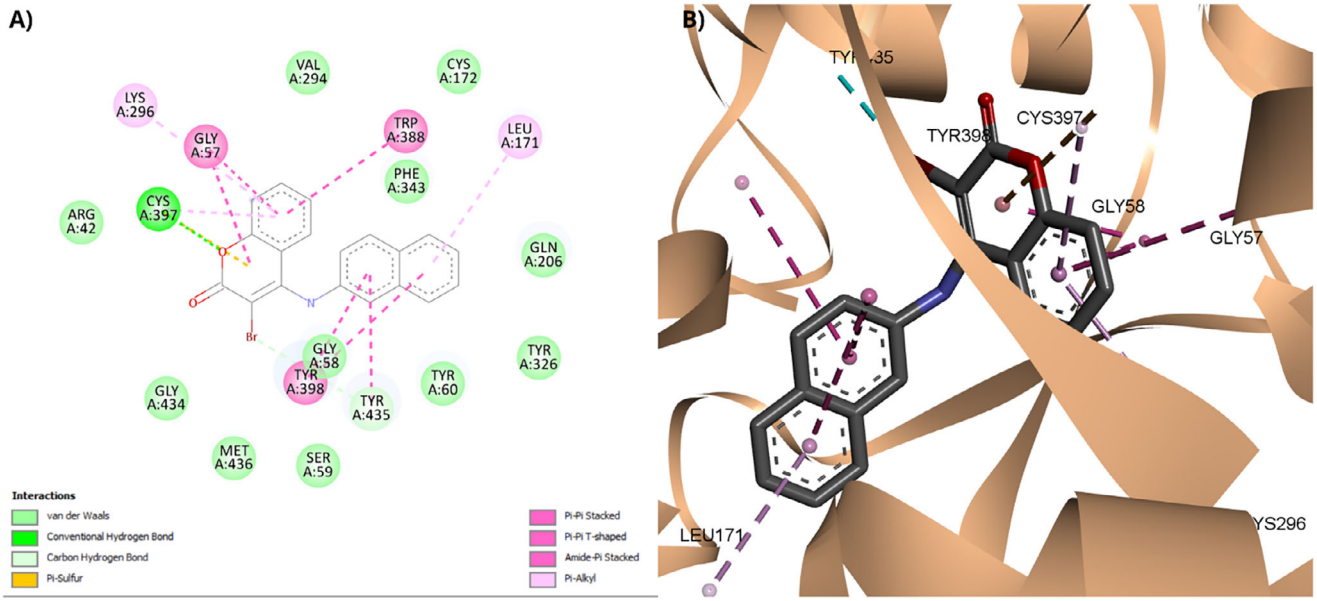

FIGURE 4 | The molecular docking results of compound **3h** are depicted as (A) protein-ligand interactions with the human MAO-B isoform in 2D format and (B) ligand-enzyme interactions in 3D format (PDB ID: 2V5Z).

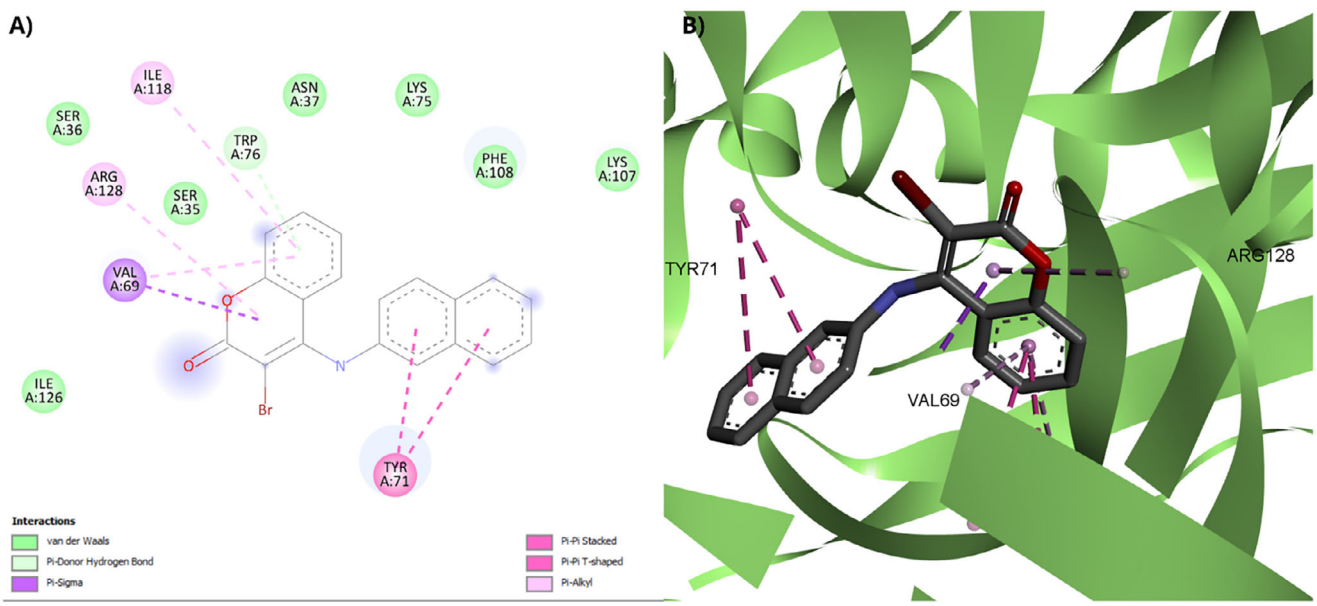

FIGURE 5 | The molecular docking results of compound **3h** are represented by (A) protein-ligand interactions with the human BACE enzyme in 2D format and (B) ligand-enzyme interactions in 3D format (PDB ID: 2WJO).

Docking studies have revealed that the analyzed compounds are potential multifunctional candidates for the treatment of neurodegenerative diseases, such as AD. This potential is attributed to their ability to interact with various biological targets, including AChE, MAO-B, BACE, and the NMDAR, achieving results equal to or surpassing those of all tested positive controls. Based on binding energy scores from docking studies, we have chosen compound **3h** (which had the lowest binding energies) as the most promising molecule for modulating the different protein targets studied, indicating its potential as a multi-target compound. Nevertheless, other molecules such as **3c**, **3g**, and **8e** also showed noteworthy results in this study.

2.6 | Prediction of ADMET Properties

Considering molecular docking findings, compounds identified as having the greatest potential to interact with different target proteins involved in AD (**3c**, **3g**, **3h,** and **8e)** were subsequently selected for further evaluation of their pharmacokinetic parameters and toxicity to predict their ADMET profiles. The results of these analyses are summarized in Table 3.

The Caco-2 permeability coefficient and human intestinal absorption metrics showed high permeability and absorption rates above 90% for compounds **3c**, **3g**, **3h,** and **8e**, indicating favorable

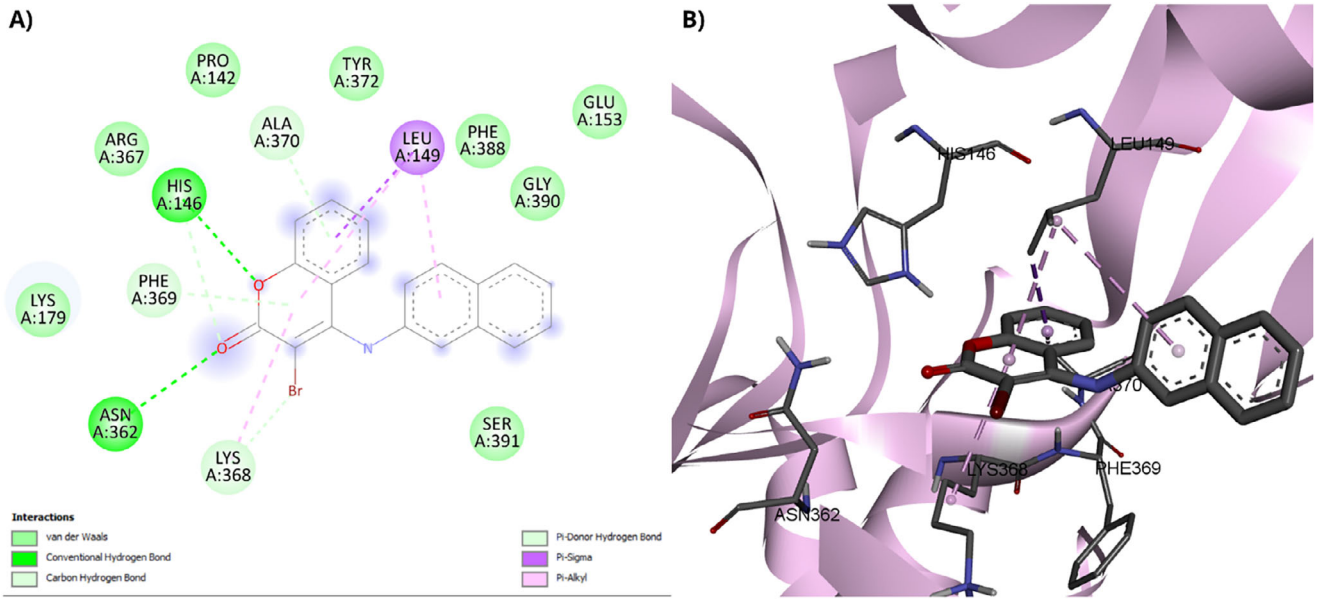

FIGURE 6 | The results of molecular docking of compound **3h** are represented by (A) protein-ligand interactions with the NMDAR receptor in 2D format and (B) ligand-receptor interactions in 3D format (PDB ID: 5EWJ).

TABLE 3 | Predicted pharmacokinetic and toxicity profiles (ADMET) of the selected compounds.

Property	Model name	Predicted value/Compound				Unit
		3c	3g	3h	8e	
Abs	Water solubility	−5.060	−5.060	−4.622	−5.213	Numeric (log mol/L)
Abs	Caco2 permeability	1.624	1.624	1.578	1.632	Numeric (log Papp in 10^{-6} cm/s)
Abs	Intestinal absorption (human)	91.784	91.784	92.217	90.392	Numeric (% absorbed)
Abs	Skin Permeability	−2.649	−2.649	−2.759	−2.654	Numeric (log Kp)
Abs	P-glycoprotein I inhibitor	No	No	Yes	No	Categorical (Yes/No)
Abs	P-glycoprotein II inhibitor	No	No	Yes	No	Categorical (Yes/No)
Dist	VDss (human)	0.128	0.128	−0.020	0.083	Numeric (log L/kg)
Dist	Fraction unbound (human)	0.036	0.036	0.154	0.028	Numeric (Fu)
Dist	BBB permeability	0.355	0.355	0.277	0.343	Numeric (log BB)
Dist	CNS permeability	−1.302	−1.302	0.380	−1.302	Numeric (log PS)
Met	CYP2D6 substrate	No	No	No	No	Categorical (Yes/No)
Met	CYP2D6 inhibitor	No	No	No	No	Categorical (Yes/No)
Exc	Total Clearance	−0.229	−0.211	−0.277	−0.139	Numeric (log ml/min/kg)
Exc	Renal OCT2 substrate	No	No	No	No	Categorical (Yes/No)
Tox	Max. tolerated dose (human)	0.158	0.158	0.709	0.162	Numeric (log mg/kg/day)
Tox	hERG I inhibitor	No	No	No	No	Categorical (Yes/No)
Tox	Oral Rat Acute Toxicity (LD_{50})	2.124	2.124	2.503	2.159	Numeric (mol/kg)
Tox	Oral Rat Chronic Toxicity (LOAEL)	0.815	0.815	1.804	0.942	Numeric (log mg/kg_bw/day)
Tox	Hepatotoxicity	No	No	Yes	No	Categorical (Yes/No)
Tox	Skin Sensitisation	No	No	No	No	Categorical (Yes/No)

Abbreviations: ADMET, absorption, distribution, metabolism, excretion, and toxicity; Papp, apparent permeability coefficient; Kp, skin permeability constant; VDss, Steady-state volume of distribution; Fu, fraction unbound; BBB, blood–brain barrier; BB, blood–brain; CNS, central nervous system; PS, permeability-surface area; LD, lethal dose; LOAEL, lowest-observed-adverse-effect level.

absorption. Metabolically, the compounds were neither substrates nor inhibitors of CYP2D6, reducing the risks of drug interactions. For excretion, these compounds are not OCT2 substrates, minimizing the risks of adverse renal interactions. Although molecular docking studies identified compound **3h** as the most promising among those tested, it is important to note that ADMET testing revealed some disadvantages of this compound compared with the others. Compound **3h** inhibited P-glycoproteins, while compounds **3c**, **3g**, and **8e** did not, suggesting that the latter may have more sustained intracellular activity. Compounds **3c**, **3g**, and **8e** are predicted to cross the blood-brain barrier (BBB), crucial for central nervous system (CNS) activity, with compound **3h** showing almost significant permeability. On the other hand, inhibiting P-glycoprotein at the BBB could enhance drug (**3h**) penetration into the CNS, although this approach carries some risks.

Throughout drug development, one common adverse effect that often causes drug failures is cardiac arrhythmias. This issue is usually linked to the drug's ability to block the hERG cardiac potassium channel [64]. Toxicity analysis via pkCSM indicated compounds **3c**, **3g**, **3h**, and **8e** did not fit as hERG inhibitors or skin sensitization agents. Besides, they present similar acute LD_{50}. On the other hand, the in silico findings also indicated that compound **3h** is predicted to have hepatotoxicity and higher chronic toxicity compared to compounds **3c**, **3g**, and **8e**. Nonetheless, given the limitations of in silico studies and the complexity of living systems, future in vitro and in vivo studies will be crucial for elucidating the mechanisms of action of these compounds, assessing their efficacy, and evaluating the potential for adverse effects. Furthermore, the potential effects of its metabolites cannot be ruled out.

3 | Conclusion

In summary, we have presented an efficient and greener methodology for the synthesis of C3-halogenated 4-aminocoumarins using trihaloisocyanuric acids. This new protocol was amenable for bromination and chlorination of several 4-aminocoumarins but showed very narrow application for the iodination of these compounds. Substrates with different structural characteristics were able to provide the corresponding halogenated products under the optimized reaction conditions, especially for bromination. The reaction scope showed good tolerance of electron-withdrawing groups (compounds **3d–f** and **8c–e**) and electron-donating groups (compounds **3b-c**, **3g**, **5**, **7,** and **8b**). A sterically hindered group attached to the nitrogen on C4 was also tolerated in the bromination reaction (compound **3h**), as well as an alkyl group (compound **7**) and the absence of any substituent at the nitrogen (compound **5**). Reactions with TICA demonstrated poor reproducibility, and the desired iodinated products were obtained only in a few cases, always in low yields. The features of this new synthetic protocol show good overlap with some of the principles of green chemistry, which are: i) no excess reagents (PII); ii) clean solvent (ethyl acetate) (PIV), iii) the reaction takes place at room temperature (PVI). We can say that the methodology has environmental advantages over conventional protocols, as it reduces the use of toxic reagents and simplifies reaction conditions. Molecular docking analysis revealed that compound **3h**, a member of the 2-chromen-2-one class, exhibited the most promising predicted interaction profile against Alzheimer's disease-related proteins among the molecules tested, although compounds **3c**, **3g**, and **8e** also demonstrated favorable results (target affinity) with favorable ADMET profiles and CNS permeability. The potential binding of the compound **3h** to targets such as AChE, MAO-B, BACE, and NMDAR suggests a multifaceted mechanism of action, with inhibitory effects on key enzymes and antagonism of glutamatergic signaling via NMDAR. These properties indicate the potential of halogenated 4-aminocoumarins as therapeutic candidates for the management of neurodegenerative disorders, particularly Alzheimer's disease.

4 | Experimental Section

4.1 | Chemistry

4.1.1 | General Remarks

Starting materials and reagents were obtained from commercial suppliers and used without further purification unless otherwise noted. Technical-grade solvents were purified by distillation before use (hexane, ethyl acetate, dichloromethane, and methanol), and PA-grade solvents were used without further purification. Reaction monitoring and retention factor (Rf) determination were performed on pre-coated thin layer chromatography (TLC) sheets (TLC SILICA GEL 60 F254, MERCK) which were visualized by ultraviolet light quenching (λ_{max} = 254 nm) or by immersion in vanillin. Developing solution, followed by heating the plate to blot out the stains. Flash column chromatography was performed on silica gel (Silica gel 60, MACHEREY-NAGEL, 230-400 mesh particle size). The results of the reaction products were determined by proton nuclear magnetic resonance spectroscopy (^{1}H NMR) and carbon nuclear magnetic resonance spectroscopy (^{13}C NMR) and were recorded on a Bruker AVANCE DRX-200 (200 MHz) or Bruker AVANCE DRX- 400 (400 MHz). Infrared (IR) spectra were recorded on an ABB FTIR-FTLA2000 spectrometer using KBr pellets. High-resolution mass spectra (HRMS) were recorded on a Bruker microTOF-Q II or Waters Xevo G2-S QTOF mass spectrometer using electrospray ionization (ESI) in positive (+) ion mode. The mass error (deviation, in ppm) of the measurements was determined by the difference between the experimentally observed m/z and the theoretical m/z.

4.2 | Synthetic Procedures

Compounds **1a-h** [65], **4** [65], and **6** [64] were synthesized according to procedures described in the literature, and their characterization corroborated the reported spectroscopic data [65–67].

4.2.1 | General Procedure for the Synthesis of 3-Bromo-4-Aminocoumarins (3a–h)

In a test tube equipped with a magnetic stirring bar, 16 mg (35 μmol) of TBCA and 1 mL of ethyl acetate were combined

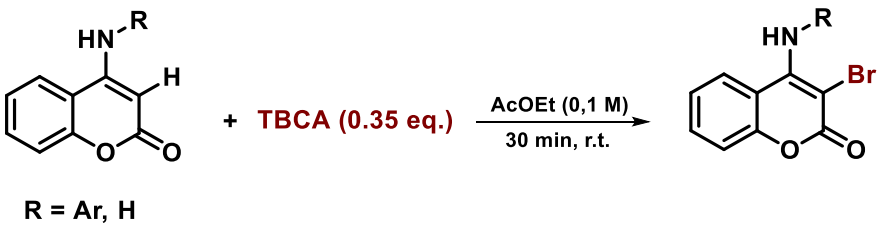

SCHEME 9 | Synthesis of 3-bromo-4-aminocoumarins (**3a–h**).

(Scheme 9). The mixture was stirred for five minutes until most of the solids dissolved. Subsequently, 0.1 mmol of the corresponding 4-aminocoumarin was added in a single portion. The reaction was allowed to proceed at room temperature for 30 min before 10 mL of ethyl acetate was added to quench the reaction. The solvent was then removed under reduced pressure, and the final product was purified via column chromatography on silica gel, using a 2:8 mixture of ethyl acetate and hexane as the mobile phase. All compounds of this series are new.

4.2.1.1 | 3-Bromo-4-(phenylamino)-2*H*-chromen-2-one (3a).

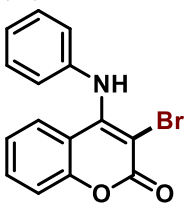

Yield: 96% (30 mg); **Physical Appearance**: light yellow solid; **mp**: 166-167°C; **^{1}H NMR (**400 MHz, $CDCl_3$) δ 7.40 (ddd, J = 8.6, 7.1, 1.6 Hz, 1H), 7.33 – 7.26 (m, 3H), 7.18 – 7.11 (m, 2H), 7.05 – 7.00 (m, 2H), 6.91 (tt, J = 7.0, 1.3 Hz, 1H). **^{13}C NMR (**100 MHz, $CDCl_3$) δ 158.1, 152.7, 149.9, 140.6, 131.9, 129.7, 125.9, 125.9, 123.4, 123.3, 117.6, 114.0, 94.4. **HRMS** (APPI$^+$): $[M-H]^-$ = 313.9822, found for $[C_{15}H_9BrNO_2]^-$ = 313.9817.

4.2.1.2 | 3-Bromo-4-((4-methoxyphenyl)amino)-2*H*-chromen-2-one (3b).

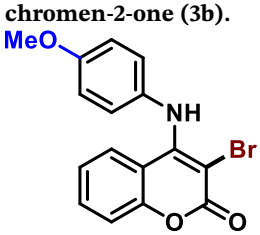

Yield: 96% (33 mg); **Physical Appearance**: brown solid; **mp**: 160–163°C; **^{1}H NMR** (400 MHz, $CDCl_3$) δ 7.42 (ddd, J = 8.5, 7.2, 1.6 Hz, 2H), 7.30 (dd, J = 8.4, 1.3 Hz, 1H), 7.12 (dd, J = 8.3, 1.5 Hz, 1H), 7.07 – 7.03 (m, 2H), 6.92 (ddd, J = 8.4, 7.2, 1.3 Hz, 1H), 6.88 – 6.84 (m, 2H), 3.80 (s, 3H). **^{13}C** NMR (100 MHz, $CDCl_3$) δ 158.2, 158.1, 152.8, 150.3, 133.2, 131.8, 125.9, 125.7, 123.2, 117.6, 114.9, 113.9, 92.2, 55.6. **HRMS** (APPI$^+$): $[M+Na]^+$ = 367.9893, found for $[C_{16}H_{12}BrNO_3Na^+]$ = 367.9890.

4.2.1.3 | 3-Bromo-4-(4-tolylamino)-2*H*-chromen-2-one (3c).

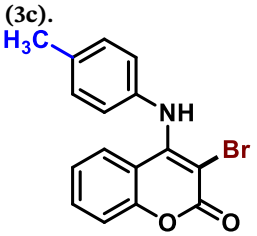

Yield: 42% (12 mg); **Physical Appearance**: brown solid; **mp**: 155-156°C; **^{1}H NMR** (400 MHz, $CDCl_3$) δ 7.43 (ddd, J = 8.6, 7.2, 1.5 Hz, 1H), 7.31 (dd, J = 8.4, 1.3 Hz, 1H), 7.19 – 7.10 (m, 3H), 6.99 – 6.93 (m, 3H), 2.34 (s, 3H). **^{13}C NMR** (10 MHz, $CDCl_3$) δ 158.2, 152.7, 150.1, 137.9, 136.1, 131.8, 130.3, 125.9, 123.7, 123.2, 117.6, 114.0, 93.4, 21.0. **HRMS** (APPI$^+$): $[M+H]^+$ = 330.0124, found for $[C_{16}H_{13}BrNO_2]^+$ = 330.0126.

4.2.1.4 | 3-Bromo-4-((4-fluorophenyl)amino)-2*H*-chromen-2-one (3d).

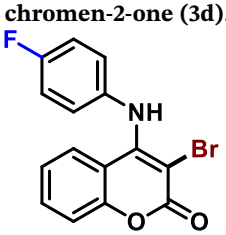

Yield: 60% (20 mg); **Physical Appearance**: white solid; **mp**: 186-187°C; **^{1}H NMR** (400 MHz, $CDCl_3$) δ 7.41 (ddd, J = 8.6, 7.2, 1.6 Hz, 1H), 7.29 (dd, J = 8.4, 1.3 Hz, 1H), 7.07 (dd, J = 8.3, 1.5 Hz, 1H), 7.03 – 6.99 (m, 3H), 6.93 (ddd, J = 8.4, 7.2, 1.3 Hz, 1H), 6.87 (d, J = 5.7 Hz, 1H). **^{13}C NMR** (101 MHz, $CDCl_3$) δ 161.9, 159.4, 158.0, 151.3 (d, J_{C-F} = 287.5 Hz), 136.6, 132.0, 125.6, 125.5 (d, J_{C-F} = 8.5 Hz), 123.4, 117.7, 116.6 (d, J_{C-F} = 23 Hz), 113.8, 94.1; **HRMS** (APPI$^+$): $[M+Na]^+$ = 355.9693, found for $[C_{15}H_9BrFNO_2Na]^+$ = 355.9697.

4.2.1.5 | 3-Bromo-4-((4-bromophenyl)amino)-2*H*-chromen-2-one (3e).

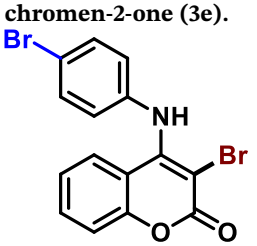

Yield: 82% (32 mg); **Physical Appearance**: yellow solid; **mp**: 194-195°C; **^{1}H NRM** (400 MHz, $CDCl_3$) δ (ppm): δ 7.54 – 7.51 (m, 1H), 7.49 – 7.46 (m, 1H), 7.38 (dd, J = 8.3, 1.0 Hz, 1H), 7.21 (dd, J

= 8.2, 1.5 Hz, 1H), 7.06 (dd, J = 11.3, 4.2 Hz, 1H), 6.97 (d, J = 8.8 Hz, 2H), 6.86 (s, 1H); **^{13}C NRM** (100 MHz, $CDCl_3$) δ 157.9, 153.2, 149.7, 139.5, 133.1, 131.9, 125.6, 124.5, 123.6, 118.6, 117.0, 114.1, 96.0; **HRMS** (APPI$^+$): $[M\text{-}H]^-$ = 391.8927, found for $[C_{15}H_8Br_2NO_2]^-$ = 391.8943.

4.2.1.6 | 3-Bromo-4-((4-chlorophenyl)amino)-2*H*-chromen-2-one (3f).

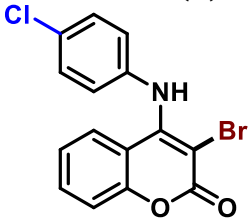

Yield: 91% (32 mg); **Physical Appearance**: brown solid; **mp**: 195-196°C; **^{1}H NMR** (400 MHz, $CDCl_3$) δ 7.51 (ddd, J = 8.6, 7.1, 1.6 Hz, 1H), 7.38 (dd, J = 8.5, 1.2 Hz, 1H), 7.36 – 7.30 (m, 2H), 7.20 (dd, J = 8.2, 1.5 Hz, 1H), 7.09 – 6.99 (m, 3H), 6.89 (s, 1H). **^{13}C NMR** (100 MHz, $CDCl_3$) δ 157.9, 152.7, 149.5, 139.2, 132.1, 131.1, 129.8, 125.6, 124.3, 123.5, 117.7, 113.9, 95.4. **HRMS** (APPI$^+$): $[M\text{-}H]^-$ = 347.9427, found for $[C_{15}H_8BrClNO_2]^-$ = 347.9433.

4.2.1.7 | 3-Bromo-4-(2-tolylamino)-2*H*-chromen-2-one (3g).

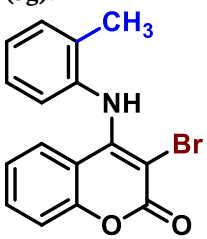

Yield: 98%; **Physical Appearance**: yellow solid**; mp**: 179-180°C**; ^{1}H NRM** (400 MHz, $CDCl_3$) δ (ppm): δ 7.46 (t, J = 7.0 Hz, 1H), 7.38 – 7.31 (m, 2H), 7.23 (t, J = 7.2 Hz, 1H), 7.16 (t, J = 7.6 Hz, 1H), 7.04 (d, J = 9.7 Hz, 1H), 6.95 (dd, J = 13.9, 7.0 Hz, 2H), 6.80 (s, 1H), 2.37 (s, 3H); **^{13}C NRM** (100 MHz, $CDCl_3$) δ 158.2, 152.5, 150.6, 138.8, 132.5, 132.0, 131.5, 127.3, 127.0, 125.6, 125.1, 123.3, 117.9, 114.1, 92.5, 18.1**; HRMS** (APPI$^+$): $[M+Na]^+$ = 351.9943, found for $[C_{16}H_{12}BrNO_2Na]^+$ = 351.9946.

4.2.1.8 | 3-Bromo-4-(naphthalen-2-ylamino)-2*H*-chromen-2-one (3h).

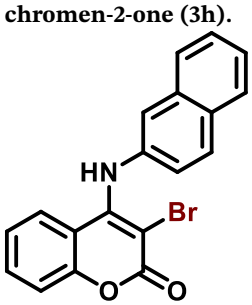

Yield: 55% (20 mg); **Physical Appearance**: brown solid; **mp**: 177-179°C; **^{1}H NRM** (400 MHz, $CDCl_3$) δ (ppm): δ 8.31 (s, 1H), 7.90 (s, 1H), 7.44 (d, J = 6.1 Hz, 6H), 7.39 (d, J = 8.3 Hz, 3H), 7.24 – 7.18 (m, 1H), 7.01 (s, 2H), 5.89 (s, 1H); **^{13}C NRM** (400 MHz, $CDCl_3$) δ (ppm): 158.5, 152.8, 149.6, 137.8, 133.8, 131.8, 129.8, 128.0, 127.4, 127.2, 126.0, 125.9, 123.7, 122.4, 120.3, 117.7, 94.7; **HRMS** (APPI$^+$): $[M\text{-}H]^-$ = 363.9973, found for $[C_{19}H_{11}BrNO_2]^-$ = 363.9981.

4.2.1.9 | 4-(Benzylamino)-3-bromo-2*H*-chromen-2-one (7).

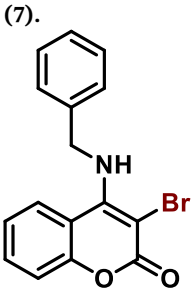

Yield: 72% (24 mg); **Physical Appearance**: White solid; **mp:** °C; **^{1}H NMR** (400 MHz, $CDCl_3$) δ 7.82 (dd, J = 8.3, 1.5 Hz, 1H), 7.56 (ddd, J = 8.6, 7.2, 1.4 Hz, 1H), 7.46 – 7.35 (m, 6H), 7.28 – 7.22 (m, 1H), 5.66 (t, J = 6.0 Hz, 1H), 4.96 (d, J = 5.9 Hz, 2H). **^{13}C NMR** (100 MHz, $CDCl_3$) δ 158.3, 153.2, 152.6, 137.5, 132.1, 129.3, 128.4, 127.3, 124.0, 123.8, 118.0, 114.4, 89.1, 51.7. HRMS (APPI$^+$): $[M+Na]^+$ = 351.9949, found for $[C_{16}H_{12}BrNO_2Na^+]$ = 351.9945

4.2.1.10 | 4-Amino-3-bromo-2*H*-chromen-2-one (5).

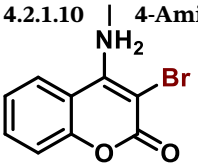

Yield: 77% (18 mg); **Physical Appearance**: White solid; **mp**: > 200°C; **^{1}H NMR (**400 MHz, DMSO-d_6) δ 8.20 – 8.13 (m, 1H), 7.64 (td, J = 7.7, 1.5 Hz, 1H), 7.40 – 7.32 (m, 2H). **^{13}C NMR** (100 MHz, DMSO-d_6) δ 158.0, 152.6, 152.2, 132.9, 124.4, 123.9, 117.3, 114.1, 81.8; **HRMS** (APPI$^+$): $[M+H]^+$ = 239.9660, found for $[C_9H_7BrNO_2]^+$ = 239.9658.

4.2.2 | General Procedure for the Synthesis of 3-chloro-4-aminocoumarins (8a–e)

In a test tube equipped with a magnetic stirring bar, 8mg (35 µmol) of TCCA and 1 mL of ethyl acetate were combined (Scheme 10). The mixture was stirred for five minutes until most of the solids dissolved. Subsequently, 0.1 mmol of the corresponding 4-aminocoumarin was added in a single portion. The reaction was allowed to proceed at room temperature for 30 min before 10 mL of ethyl acetate was added to quench the reaction. The solvent was then removed under reduced pressure, and the final product was purified via column chromatography on silica gel, using a 2:8 mixture of ethyl acetate and hexane as the mobile phase. All compounds of this series are new.

4.2.2.1 | 3-Chloro-4-(phenylamino)-2*H*-chromen-2-one (8a).

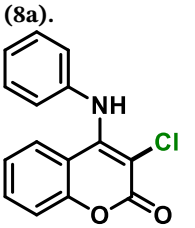

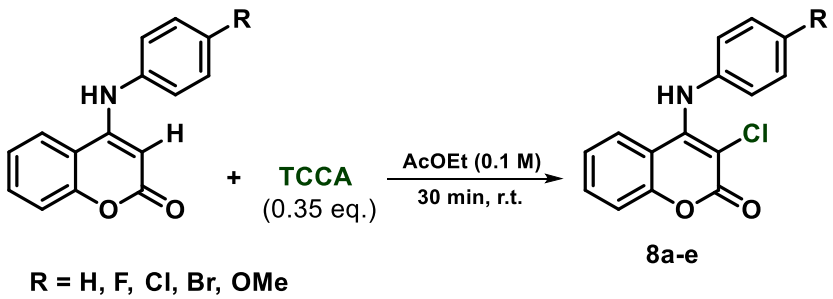

SCHEME 10 | Synthesis of 3-chloro-4-aminocoumarins (**8a–e**).

Yield: 43% (12 mg); **Physical Appearance**: yellow solid; **mp**: 187-188°C; **^{1}H NMR (**400 MHz, $CDCl_3$) δ 7.47 (ddd, J = 8.6, 7.2, 1.5 Hz, 1H), 7.39 – 7.34 (m, 3H), 7.28 – 7.20 (m, 2H), 7.14 – 7.06 (m, 2H), 7.01 (ddd, J = 8.3, 7.2, 1.3 Hz, 1H). **^{13}C NMR** (100 MHz, $CDCl_3$) δ 158.1, 152.2, 147.8, 140.4, 131.8, 129.6, 125.8, 125.8, 123.4, 123.4, 117.6, 114.2, 102.7. **HRMS** (APPI$^+$): $[M-H]^-$ = 270.0327, found for $[C_{15}H_9ClNO_2]^-$ = 270.0326.

4.2.2.2 | 3-Chloro-4-((4-methoxyphenyl)amino)-2*H*-chromen-2-one (8b).

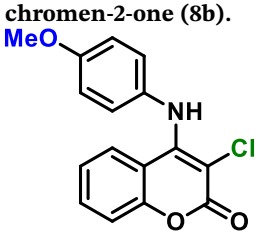

Yield: 55%; **Physical Appearance**: brown solid; **mp**: 174-175°C; **^{1}H NMR** (400 MHz, $CDCl_3$) δ 7.45 (ddd, J = 8.6, 7.2, 1.5 Hz, 1H), 7.35 (dd, J = 8.4, 1.3 Hz, 1H), 7.16 (dd, J = 8.3, 1.5 Hz, 1H), 7.13 – 7.05 (m, 2H), 6.99 (ddd, J = 8.4, 7.1, 1.3 Hz, 1H), 6.96 – 6.89 (m, 2H), 3.85 (s, 3H). **^{13}C NMR** (100 MHz, $CDCl_3$) δ 158.1, 152.3, 148.3, 133.0, 131.6, 125.9, 125.7, 123.3, 117.7, 114.9, 114.0, 100.7, 55.6. **HRMS** (APPI$^+$): $[M-H]^-$ = 300.0433, found for $[C_{16}H_{11}ClNO_3]^-$ = 300.0440.

4.2.2.3 | 3-Chloro-4-((4-fluorophenyl)amino)-2*H*-chromen-2-one (8c).

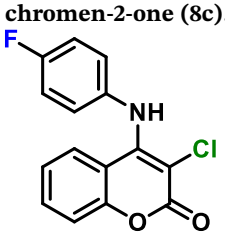

Yield: 82% (24 mg); **Physical Appearance**: brown solid; **mp**: 117-119°C; **^{1}H NMR** (400 MHz, DMSO-d_6) δ 9.24 (s, 1H), 7.83 (dd, J = 8.2, 1.5 Hz, 1H), 7.64 (ddd, J = 8.6, 7.2, 1.4 Hz, 1H), 7.44 (dd, J = 8.3, 1.2 Hz, 1H), 7.37 – 7.28 (m, 1H), 7.23 – 7.08 (m, 4H). **^{13}C NMR** (100 MHz, DMSO-d_6) δ 160.5, 158.5, 158.1, 151.7, 147.6, 137.1, 137.1, 132.6, 125.1, 125.0, 124.6, 124.4, 117.5, 116.3, 115.8, 115.6, 100.0. **HRMS** (APPI$^+$): $[M-H]^-$ = 288.0228, found for $[C_{15}H_8ClFNO_2]^-$ = 288.0226.

4.2.2.4 | 4-((4-Bromophenyl)amino)-3-chloro-2*H*-chromen-2-one (8d).

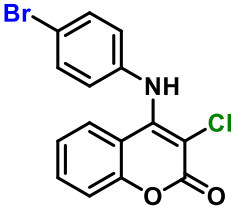

Yield: 77% (27 mg); **Physical Appearance**: beige solid; **mp**: > 200°C; **^{1}H NMR** (400 MHz, DMSO-d_6) δ 9.30 (s, 1H), 7.84 (dd, J = 8.2, 1.5 Hz, 1H), 7.65 (ddd, J = 8.6, 7.2, 1.5 Hz, 1H), 7.51 – 7.44 (m, 3H), 7.35 (ddd, J = 8.3, 7.2, 1.2 Hz, 1H), 7.05 – 6.97 (m, 2H). **^{13}C NMR** (100 MHz, DMSO-d_6) δ 158.4, 151.7, 147.1, 140.4, 132.7, 131.8, 124.8, 124.6, 124.1, 117.5, 116.6, 115.6, 102.3. **HRMS** (APPI$^+$): $[M-H]^-$ = 347.9432, found for $[C_{15}H_8BrClNO_2]^-$ = 347.9433.

4.2.2.5 | 3-Chloro-4-((4-chlorophenyl)amino)-2*H*-chromen-2-one (8e).

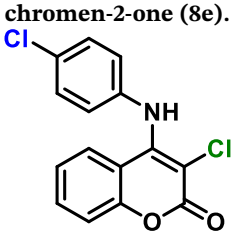

Yield: 62% (27 mg); **Physical Appearance**: brown solid; **mp**: 121-122°C; **^{1}H NMR** (400 MHz, DMSO-d_6) δ 9.32 (s, 1H), 7.84 (dd, J = 8.2, 1.5 Hz, 1H), 7.65 (ddd, J = 8.6, 7.2, 1.5 Hz, 1H), 7.46 (dd, J = 8.3, 1.2 Hz, 1H), 7.38 – 7.34 (m, 3H), 7.15 – 7.00 (m, 2H). **^{13}C NMR** (100 MHz, DMSO-d_6) δ 158.4, 151.7, 147.2, 139.9, 132.7, 128.9, 127.7, 124.7, 124.5, 123.8, 117.5, 116.5, 102.0. **HRMS** (APPI$^+$): $[M-H]^-$ = 303.9932, found for $[C_{15}H_8Cl_2NO_2]^-$ = 303.9939.

4.2.3 | General Procedure for the Synthesis of 3-iodo-4-aminocoumarins (10a-b)

In a test tube equipped with a magnetic stirring bar, TICA (17,7 mg, 35 μmol) was dissolved in ethyl acetate (1 mL), and the mixture was stirred for five minutes until most of the solid dissolved (Scheme 11). Subsequently, the corresponding 4-aminocoumarin (0.1 mmol) was added in a single portion. The reaction mixture was stirred at room temperature for 30 min, after which ethyl acetate (10 mL) was added to quench the reaction,

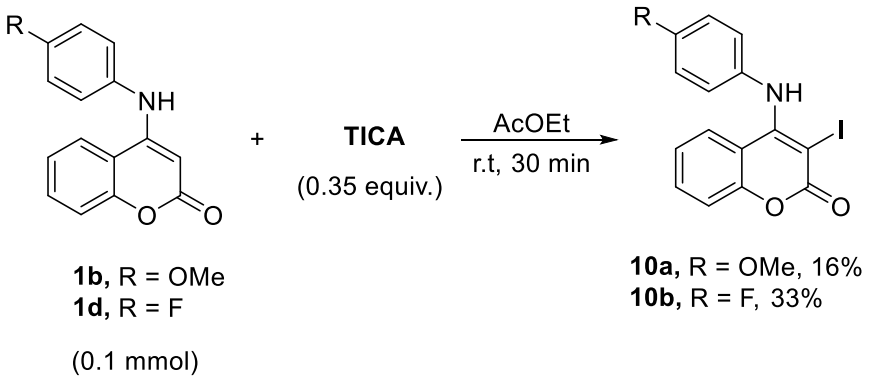

SCHEME 11 | Synthesis of 3-iodo-4-aminocoumarins (**10a-b**).

and the solvent was then removed under reduced pressure. The crude product was purified by flash column chromatography on silica gel using a gradient of ethyl acetate/hexane (10:90 → 30:70) as the mobile phase. Both compounds of this series are new.

4.2.3.1 | 3-Iodo-4-(4-methoxyphenyl)amino)-2*H*-chromen-2-one (10a).

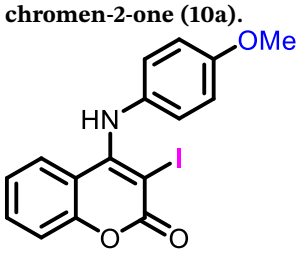

Yield: 16% (6 mg); **Physical Appearance**: brown solid; **^{1}H NMR** (400 MHz, $CDCl_3$) δ 7.44 (d, J = 8.4 Hz, 1H), 7.35 (d, J = 21.2 Hz, 2H), 7.17 (t, 1H), 7.06 (d, J = 6.9 Hz, 5H), 6.92 – 6.86 (m, 8H), 3.83 (s, 3H).**^{13}C NMR** (100 MHz, $CDCl_3$) δ 159.3, 158.3, 153.9, 153.2, 135.3, 133.9, 133.2, 132.5, 125.7, 123.0, 117.4, 114.4, 113.2, 55.7, 29.9. (APPI$^+$): $[M+Na]^+$ = 415.9754, found for $[C_{16}H_{12}INNaO_3]^+$ = 415.9759.

4.2.3.2 | 3-Iodo-4-(4-fluorophenylamino)-2*H*-chromen-2-one (10b).

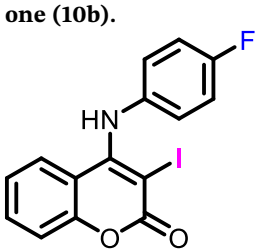

Yield: 33% (12 mg); **Physical Appearance**: brown solid; **^{1}H NMR** (400 MHz, $CDCl_3$) δ 7.51 – 7.44 (m, 1H), 7.37 (d, J = 9.1 Hz, 1H), 7.15 (d, J = 9.7 Hz, 1H), 7.07 (s, 4H), 7.00 – 6.95 (m, 1H), 6.81 (s, 1H). **^{13}C NMR** (100 MHz, $CDCl_3$) δ 157.9, 152.5, 150.3, 140.4, 132.2, 129.4, 125.8, 123.0, 117.6, 114.4, 94.4. **HRMS** (APPI$^+$): $[M+H]^+$ = 381.9735, found for $[C_{15}H_{10}FINO_2]^+$ = 381.9695.

4.3 | Molecular Docking

Molecular docking was used as a crucial tool to predict the optimal orientation and binding with the AChE, MAO-B, BACE, and NMDAR. This technique enabled the simulation and analysis of the interactions between the tested compounds and the target proteins. Additionally, positive controls were analyzed for comparison (Rivastigmine—AChE, Verubecestat—BACE, Selegiline—MAO-B, Memantine—NMDAR).

Initially, the 2D structures of the compounds were drawn using ChemDraw software and then converted to 3D using Avogadro 0.9.4 [68]. The electric charges of each atom and the types and numbers of torsions were defined using AutoDock Tools [69]. The 3D crystal structures of the protein binding sites were obtained from the Protein Data Bank (PDB): AChE (PDB ID: 4PQE), MAO-B (PDB ID: 2V5Z), BACE (PDB ID: 2WJO), and NMDAR-subunits GluN1/GluN2B (PDB ID: 5EWJ). The ligands were removed from the enzyme structures using Chimera 1.5.3 [70]. The enzyme preparation, which involved the removal of water molecules and ions, and the correction of heterogroups, was carried out using AutoDock Tools. Docking was then performed with AutoDock Vina 1.1.1, which identifies potential interaction sites [71] The interactions between the ligands and the proteins were analyzed using Discovery Studio 2016.

4.4 | Prediction of ADMET Properties

The pharmacokinetic properties encompassing the absorption, distribution, metabolism, excretion, and toxicity (ADMET) of selected compounds were assessed using the pkCSM ADMET website developed by Accelrys Software, Inc. in San Diego, CA, United States [72]. Absorption assessment involved using the Caco-2 cell line to simulate membrane permeability and predict intestinal and dermal absorption. Additionally, we investigated the compounds' interactions with P-glycoprotein (P-gp), considering their role as substrates or inhibitors. Compound distribution was evaluated for its ability to cross the blood-brain barrier and permeate the CNS using appropriate computational models. The volume of distribution (VDss) was predicted to estimate tissue distribution. Regarding metabolism, we employed cytochrome P450 (CYP) enzyme models to predict whether the compounds act as substrates or inhibitors of these enzymes. Excretion was estimated by considering renal transport via organic cation transporter 2 (OCT2) using a total clearance model. Toxicity evaluation included computational predictions, the ability to inhibit the hERG potassium channel, and risks of hepatotoxicity and dermal sensitization.

Author Contributions

Maryelle A.G. de Carvalho, Vinicius C. Alves, Lara M. Flores and Carlos V. Doerner performed all the experimental work. Tácia K. Hall and Cristiani F. Bortolatto performed all the computational work. Louis P. Sandjo, José S. S. Neto, Antonio L. Braga and Francisco F. de Assis contributed to the mentorship of the work.

Acknowledgments

The authors thank CAPES (grant No 633/2020), CNPq (404172/2023-7, 444559/2024-8 and 402548/2024-8) and FAPESC (2024TR002635) for the financial support. MAGC, also thanks CAPES for the fellowship. The authors also acknowledge UFSC and UFPB for the infrastructure, LAM-RMN for the NMR analyses, LabCroMS, CentralCROM and PPGBTox (UFSM) for the MS and HRMS analyses.

The Article Processing Charge for the publication of this research was funded by the Coordenação de Aperfeiçoamento de Pessoal de Nível Superior - Brasil (CAPES) (ROR identifier: 00x0ma614).

Conflicts of Interest

The authors declare no conflicts of interest.

Data Availability Statement

The data that support the findings of this study are available from the corresponding author upon reasonable request.

References

1. A. Stefanachi, F. Leonetti, L. Pisani, M. Catto, and A. Carotti, "Coumarin: A Natural, Privileged and Versatile Scaffold for Bioactive Compounds," *Molecules (Basel, Switzerland)* 23, no. 2 (2018): 250, https://doi.org/10.3390/molecules23020250.

2. K. N. Venugopala, V. Rashmi, and B. Odhav, "Review on Natural Coumarin Lead Compounds for Their Pharmacological Activity," *BioMed Research International* 2013, no. 1 (2013): 963248, https://doi.org/10.1155/2013/963248.

3. S. D. Sarker and L. Nahar, "Progress in the Chemistry of Naturally Occurring Coumarins," *Progress in the Chemistry of Organic Natural Products* 106 (2017): 241–304, https://doi.org/10.1007/978-3-319-59542-9_3.

4. F. Annunziata, C. Pinna, S. Dallavalle, L. Tamborini, and A. Pinto, "An Overview of Coumarin as a Versatile and Readily Accessible Scaffold with Broad-Ranging Biological Activities," *International Journal of Molecular Sciences* 21, no. 13 (2020): 4618, https://doi.org/10.3390/ijms21134618.

5. C. S. Kumar, D. A. Daoud, S. Alarifib, S. Radhakrishnana, and I. Akbar, "In Silico Molecular Docking: Evaluation of Coumarin Based Derivatives against SARS-CoV-2," *Journal of Infection and Public Health* 13 (2020): 1671–1677, https://doi.org/10.1016/j.jiph.2020.09.002.

6. T. Dettori, G. Sanna, A. Cocco, et al., "Synthesis and Antiproliferative Effect of Halogenated Coumarin Derivatives," *Molecules (Basel, Switzerland)* 27, no. 24 (2022): 8897, https://doi.org/10.3390/molecules27248897.

7. M. Sadeghpour, M. A. Olyaei, and A. Adl, "4-Aminocoumarin Derivatives: Synthesis and Applications," *New Journal of Chemistry* 45 (2021): 5744–5763, https://doi.org/10.1039/D1NJ00614B.

8. L. S. A. Carneiro, F. Almeida-Souza, Y. S. C. Lopes, et al., "Synthesis of 3-aryl-4-(*N*-aryl)aminocoumarins via Photoredox Arylation and the Evaluation of Their Biological Activity," *Bioorganic Chemistry* 114 (2021): 105141, https://doi.org/10.1016/j.bioorg.2021.105141.

9. E. A. Akl, A. J. Comerota, and P. Prandoni, "Antithrombotic Therapy for VTE Disease," *Chest* 141, no. 2 (2012): e419S–e496S, https://doi.org/10.1378/chest.11-2301.

10. X. L. Hu, C. Gao, Z. Xu, M. L. Liu, L. S. Feng, and G. D. Zhang, "Recent Development of Coumarin Derivatives as Potential Antiplasmodial and Antimalarial Agents," *Current Topics in Medicinal Chemistry* 18, no. 2 (2018): 114–123, https://doi.org/10.2174/1568026618666171215101158.

11. K. Kasumbwe, K. N. Venugopala, V. Mohanlall, and B. Odhav, "Antimicrobial and Antioxidant Activities of Substituted Halogenated Coumarins," *Journal of Medicinal Plants Research* 8, no. 5 (2014): 274–281, https://doi.org/10.5897/JMPR2013.4419.

12. G. H. Golshadi, S. Balalaie, A. Aliahmadi, and R. Moghimi, "Synthesis of 4-N-*α*-coumaryl Amino Acids and Investigation of Their Antioxidant, Antimicrobial Activities and Fluorescence Spectra," *Amino Acids* 50 (2018): 1461–1470, https://doi.org/10.1007/s00726-018-2624-5.

13. K. Kasumbwe, K. N. Venugopala, V. Mohanlall, and B. Odhav, "Synthetic Mono/Di-halogenated Coumarin Derivatives and Their Anticancer Properties," *Anti-Cancer Agents in Medicinal Chemistry* 17 (2017): 276–285, https://doi.org/10.2174/1871520616666160926112508.

14. N. Ristić, N. Radulović, B. Dekić, M. Ristić, and V. Dekić, "Synthesis and Antioxidant Activity of a New 4-aminocoumarin Derivative," *University Thought—Publication in Natural Sciences* 8 (2018): 27–32, https://doi.org/10.5937/univtho8-19770.

15. A. Aminjafari, M. Miroliaei, V. T. Angelova, et al., "Antioxidant Activity and Protective Role on Protein Glycation of Synthetic Aminocoumarins," *Electronic Journal of Biotechnology* 24 (2016): 43–48, https://doi.org/10.1016/j.ejbt.2016.08.004.

16. M. Di Braccio, G. Grossi, G. Roma, M. G. Signorello, and G. Leoncini, "Synthesis and In Vitro Inhibitory Activity on human Platelet Aggregation of Novel Properly Substituted 4-(1-piperazinyl)coumarins," *European Journal of Medicinal Chemistry* 39 (2004): 397–409, https://doi.org/10.1016/j.ejmech.2003.12.010.

17. G. Roma, M. Di Braccio, A. Carrieri, G. Grossi, M. G. S. G. Leoncini, and A. Carotti, "Coumarin, Chromone, and 4(3H)-pyrimidinone Novel Bicyclic and Tricyclic Derivatives as Antiplatelet Agents: Synthesis, Biological Evaluation, and Comparative Molecular Field Analysis," *Bioorganic & Medicinal Chemistry* 11 (2003): 123–138, https://doi.org/10.1016/S0968-0896(02)00307-3.

18. K. Tabakovic, I. Tabakovic, N. Ajdini, and O. Leci, "A Novel Transformation of 4-Arylaminocoumarins to 6 H-1-Benzopyrano[4,3-b]Quinolin-6-ones Under V ilsmeier-Haack Conditions," *Synthesis* 1987, no. 3 (1987): 308–310, https://doi.org/10.1055/s-1987-27930.

19. A. Sharma and P. Gogoi, "Transition-metal Free C(sp^2)–C(sp^2) Bond Formation: Arylation of 4-aminocoumarins Using Arynes as an Aryl Source," *Organic & Biomolecular Chemistry* 17 (2019): 9014–9025, https://doi.org/10.1039/C9OB01919G.

20. A. L. Belladona, M. C. Dilelio, R. Cargnelutti, R. T. Barcellos, C. C. Silveira, and R. F. Schumacher, "Direct and Regioselective C−H Selenylation of 4-Aminocoumarin Derivatives Mediated by Selectfluor®," *ChemistrySelect* 8 (2023): e202300377, https://doi.org/10.1002/slct.202300377.

21. D. Yang, G. Li, C. Xing, W. Cui, K. Li, and W. Wei, "Metal- and Photocatalyst-free Visible-light-promoted Regioselective Selenylation of Coumarin Derivatives *via* Oxidation-induced C–H Functionalization," *Organic Chemistry Frontiers* 5 (2018): 2974–2979, https://doi.org/10.1039/C8QO00899J.

22. G. Li, Q. Yan, X. Gong, X. Dou, and D. Yang, "Photocatalyst-Free Regioselective C–H Thiocyanation of 4-Anilinocoumarins Under Visible Light," *ACS Sustainable Chemistry & Engineering* 7 (2019): 14009–14015, https://doi.org/10.1021/acssuschemeng.9b02511.

23. M. Adib, F. Peytam, M. Rahmanian-Jazi, M. Mohammadi-Khanaposhtani, S. Mahernia, et al., "Design, Synthesis and In Vitro *α*-glucosidase Inhibition of Novel Coumarin-pyridines as Potent Antidiabetic Agents," *New Journal of Chemistry* 42 (2018): 17268–17278, https://doi.org/10.1039/C8NJ02495B.

24. S. Mukherjee, S. Sarkar, and A. Pramanik, "A Sustainable Synthesis of Functionalized Pyrrole Fused Coumarins Under Solvent-Free Conditions Using Magnetic Nanocatalyst and a New Route to Polyaromatic Indolo-

coumarins," *ChemistrySelect* 3 (2018): 1537, https://doi.org/10.1002/slct.201703146.

25. G. R. Jadhav, D. G. Deshmukh, V. J. Medhane, V. B. Gaikwad, and A. D. Bholay, "2,5-Disubstituted 1,3,4-oxadiazole Derivatives of Chromeno[4,3-b2,5-Disubstituted 1,3,4-oxadiazole derivatives of chromeno[4,3-b]Pyridine: Synthesis and Study of Antimicrobial Potency," *Heterocyclic Communications* 22 (2016): 123–130, https://doi.org/10.1515/hc-2015-0215.

26. P. Patra and S. Patra, "4-Aminocoumarin Derivatives as Multifaceted Building Blocks for the Development of Various Bioactive Fused Coumarin Heterocycles: A Brief Review," *Current Organic Chemistry* 26 (2022): 1585, https://doi.org/10.2174/1385272827666221209101112.

27. J. Pavlinac, M. Zupan, K. Laali, and S. S. Stavber, "Halogenation of Organic Compounds in Ionic Liquids," *Tetrahedron* 65, no. 29-30 (2009): 5625–5662, https://doi.org/10.1016/j.tet.2009.04.092.

28. C. H. Veisi and R. Ghorbani-Vaghei, "Recent Progress in the Application of N-halo Reagents in the Synthesis of Heterocyclic Compounds," *Tetrahedron* 66, no. 38 (2010): 7445–7463, https://doi.org/10.1016/j.tet.2010.07.015.

29. G. Cavallo, P. Metrangolo, R. Milani, et al., "The Halogen Bond," *Chemical Reviews* 116, no. 4 (2016): 2478–2601, https://doi.org/10.1021/acs.chemrev.5b00484.

30. Z. Xu, Z. Yang, Y. Liu, K. Chen, et al., "Halogen Bond: Its Role beyond Drug–Target Binding Affinity for Drug Discovery and Development," *Journal of Chemical Information and Modeling* 54, no. 1 (2014): 69–78, https://doi.org/10.1021/ci400539q.

31. S. Adak and B. S. Moore, "Cryptic Halogenation Reactions in Natural Product Biosynthesis," *Natural Product Reports* 38 (2021): 1760–1774, https://doi.org/10.1039/d1np00010a.

32. T. Huo, X. Zhao, Z. Cheng, et al., "Late-stage Modification of Bioactive Compounds: Improving Druggability Through Efficient Molecular Editing," *Acta Pharmaceutica Sinica B* 14, no. 3 (2024): 1030–1076, https://doi.org/10.1016/j.apsb.2023.11.021.

33. M. Mardirossian, M. Rubini, M. F. A. Adamo, et al., "Natural and Synthetic Halogenated Amino Acids—Structural and Bioactive Features in Antimicrobial Peptides and Peptidomimetics," *Molecules (Basel, Switzerland)* 26, no. 23 (2021): 7401, https://doi.org/10.3390/molecules26237401.

34. L. Mendez, G. Henriquez, S. Sirimulla, and M. Narayan, "Looking Back, Looking Forward at Halogen Bonding in Drug Discovery," *Molecules (Basel, Switzerland)* 22 (2017): 1397, https://doi.org/10.3390/molecules22091397.

35. C. Wagner, M. E. Omari, and G. M. König, "Biohalogenation: Nature's Way to Synthesize Halogenated Metabolites," *Journal of Natural Products* 72, no. 3 (2009): 540–553, https://doi.org/10.1021/np800651m.

36. R. Wilcken, M. O. Zimmermann, A. Lange, C. A. Joerger, and M. F. Boeckler, "Principles and Applications of Halogen Bonding in Medicinal Chemistry and Chemical Biology," *Journal of Medicinal Chemistry* 56, no. 4 (2013): 1363–1388, https://doi.org/10.1021/jm3012068.

37. P. R. S. Kodavanti, L. G. Costa, and M. Aschner, "Perspective on Halogenated Organic Compounds," *Advances in Neurotoxicology* 10 (2023): 1–25, Academic Press, https://doi.org/10.1016/bs.ant.2023.06.001.

38. ACADEMIA BRASILEIRA DE CIÊNCIAS (ABC). Nobel Prize in Medicine goesto scientists who made COVID-19 vaccines possible, http://www.abc.org.br/2023/10/02/nobel-de-medicina-vai-para-cientistas-que-possibilitaram-as-vacinas-contra-a-covid-19/ Accessed on: April 1, 2025.

39. W. S. Hamama, M. E. Ibrahim, A. E. Metwalli, et al., "Recent Synthetic Aspects on the Chemistry of Aminocoumarins," *Research on Chemical Intermediates* 43 (2017): 5943–5983, https://doi.org/10.1007/s11164-017-2973-9.

40. W. Hao and Y. Liu, "C–H Bond Halogenation Catalyzed or Mediated by Copper: An Overview," *Beilstein Journal of Organic Chemistry* 11, no. 11 (2015): 2132–2144, https://doi.org/10.3762/bjoc.11.230.

41. Y. Nishii, Y. M. Ikeda, Y. Hayashi, S. Kawauchi, and M. Miura, "Triptycenyl Sulfide: A Practical and Active Catalyst for Electrophilic Aromatic Halogenation Using *N*-Halosuccinimides," *Journal of American Chemical Society* 142, no. 3 (2020): 1621–1629, https://doi.org/10.1021/jacs.9b12672.

42. R. Semwal, C. Ravi, R. Kumar, R. Meena, and S. Adimurthy, "Sodium Salts (NaI/NaBr/NaCl) for the Halogenation of Imidazo-Fused Heterocycles," *Journal of Organic Chemistry* 84, no. 2 (2019): 792–805, https://doi.org/10.1021/acs.joc.8b02637.

43. H. Firouzabadi, N. Iiranpoor, and S. Kazeni, "Direct Halogenation of Organic Compounds With Halides Using Oxone in Water — A Green Protocol," *Canadian Journal of Chemistry* 87, no. 12 (2009): 675–1681, https://doi.org/10.1139/V09-125.

44. K. C. Naidu, O. Rikuto, N. Shotaro, M. Masahiro, et al., "Aromatic Halogenation Using Carborane Catalyst," *Chemistry (Weinheim An Der Bergstrasse, Germany)* 10, no. 1 (2024): 402–413, https://doi.org/10.1016/j.chempr.2023.10.006.

45. A. Hubbard, T. Okazaki, and K. K. Laali, "Chlorination of Aromatics With Trichloroisocyanuric Acid (TCICA) in Bronsted-Acidic Imidazolium Ionic Liquid [BMIM(SO_3H)][OTf]: An Economical, Green Protocol for the Synthesis of Chloroarenes," *Australian Journal of Chemistry* 60, no. 12 (2007): 923–927, https://doi.org/10.1071/CH07261.

46. U. Tilstam and H. Weinmann, "Trichloroisocyanuric Acid: A Safe and Efficient Oxidant," *Organic Process Research & Development* 6, no. 4 (2002): 384–393, https://doi.org/10.1021/op010103h.

47. L. T. C. Crespo, M. R. Senra, P. M. Esteves, and M. C. Matos, "Tribromoisocyanuric Acid as a Green Cohalogenating Reagent: an Efficient Transformation of Alkynes into α,α-Dibromoketones and Vicinal Dibromoalkenes," *Letters Organic Chemistry* 16, no. 8 (2019): 627–632, https://doi.org/10.2174/1570178615666180803152951.

48. S. Gaspa, M. Carraro, L. Pisano, et al., "Trichloroisocyanuric Acid: A Versatile and Efficient Chlorinating and Oxidizing Reagent," *European Journal of Organic Chemistry* (2019): 3544–3552, https://doi.org/10.1002/ejoc.201900449.

49. S. Cunha, T. Fontes, D. M. Araújo, and V. B. Riatto, "Mechanochemical Chlorination of Acetanilide", *Quimica Nova* 41(1), (2018): 116–119, https://doi.org/10.21577/0100-4042.20170138.

50. J. S. S. Neto, R. A. Balaguez, M. S. Franco, et al., "Trihaloisocyanuric Acids in Ethanol: An Eco-friendly System for the Regioselective Halogenation of Imidazo-heteroarenes," *Green Chemistry* 22, no. 11 (2020): 3410–3415, https://doi.org/10.1039/D0GC00137F.

51. C. Lemke, J. Christmann, J. Yin, et al., "Chromenones as Multineurotargeting Inhibitors of Human Enzymes," *ACS Omega* 4, no. 26 (2019): 22161–22168, https://doi.org/10.1021/acsomega.9b03409.

52. H. E. A. Hassan, H. J. Kim, K. Park, et al., "Synthesis and Biological Evaluation of O6-Aminoalkyl-hispidol Analogs as Multifunctional Monoamine Oxidase-B Inhibitors Towards Management of Neurodegenerative Diseases," *Antioxidants* 12, no. 5 (2023): 1033, https://doi.org/10.3390/antiox12051033.

53. S. H. Combe, A. Hosseini, A. Parra, and P. R. Schreiner, "Mild Aliphatic and Benzylic Hydrocarbon C–H Bond Chlorination Using Trichloroisocyanuric Acid," *Journal of Organic Chemistry* 82, no. 5 (2017): 2407–2413, https://doi.org/10.1021/acs.joc.6b02829.

54. S. Gaspa, A. Valentoni, A. Mulas, A. Porcheddu, and L. De Luca, "Metal-Free Preparation of α-H-Chlorinated Alkylaromatic Hydrocarbons by Sunlight," *ChemistrySelect* 3 (2018): 7991–7995, https://doi.org/10.1002/slct.201801168.

55. Z. Marco, A. Cherubini, S. Volpato, L. Ferruci, and G. Zulian, "Acetylcholinesterase-inhibitors Slow Cognitive Decline and Decrease Overall Mortality in Older Patients With Dementia," *Scientific Reports* 12 (2022): 12214, https://doi.org/10.1038/s41598-022-16476-w.

56. I. J. Hakeem, "Molecular Docking Analysis of Acetylcholinesterase Inhibitors for Alzheimer's Disease Management," *Bioinformation* 19, no. 5 (2023): 565–570, https://doi.org/10.6026/97320630019565.

57. L. Zhang, D. Li, F. Cao, et al., "Identification of Human Acetylcholinesterase Inhibitors From the Constituents of EGb761 by Modeling Docking and Molecular Dynamics Simulations," *Combinatorial Chemistry & High Throughput Screening* 21, no. 1 (2018): 41–49, https://doi.org/10.2174/1386207320666171123201910.

58. R. M. Geha, K. Chen, J. Wouter, F. Ooms, and J. C. Shih, "Analysis of Conserved Active Site Residues in Monoamine Oxidase A and B and Their Three-dimensional Molecular Modeling," *Journal of Biological Chemistry* 277, no. 19 (2002): 17209–17216, https://doi.org/10.1074/jbc.m110920200.

59. J. Reis, N. Manzella, F. Cagide, et al., "Tight-binding Inhibition of Human Monoamine Oxidase B by Chromone Analogs: A Kinetic, Crystallographic, and Biological Analysis," *Journal of Medicinal Chemistry* 61, no. 9 (2018): 4203–4212, https://doi.org/10.1021/acs.jmedchem.8b00357.

60. E. McDade, I. Voytyuk, P. Aisen, R. J. Bateman, et al., "The Case for Low-level BACE1 Inhibition for the Prevention of Alzheimer Disease," *Nature reviews Neurology* 17 (2021): 703–714, https://doi.org/10.1038/s41582-021-00545-1.

61. P. Mishra, P. Ray, T. Nayek, et al., "Design and Molecular Screening of Various Compounds by Molecular Docking as BACE-1 Inhibitors," *Qeios* (2024), https://doi.org/10.32388/9OCR7D.

62. A. J. Siddiqui, R. Badraoui, S. Jahan, et al., "Targeting NMDA Receptor in Alzheimer's Disease: Identifying Novel Inhibitors Using Computational Approaches," *Frontiers in Pharmacology* 14 (2023): 1208968, https://doi.org/10.3389/fphar.2023.1208968.

63. M. K. Leong, R. G. Syu, Y. L. Ding, and C. F. Weng, "Prediction of N-methyl-D-aspartate Receptor GluN1-ligand Binding Affinity by a Novel SVM-pose/SVM-score Combinatorial Ensemble Docking Scheme," *Scientific Reports* 7 (2017): 40053, https://doi.org/10.1038/srep40053.

64. A. Garrido, A. Lepailleur, S. M. Mignani, P. Dallemagne, and C. Rochais, "hERG Toxicity Assessment: Useful Guidelines for Drug Design," *European journal of medicinal chemistry* 195 (2020): 112290, https://doi.org/10.1016/j.ejmech.2020.112290.

65. Y. Weng, H. Zhou, C. Sun, Y. Xie, and W. Su, "Copper-Catalyzed Cyclization for Access to 6H-Chromeno[4,3-b]Quinolin-6-ones Employing DMF as the Carbon Source," *Journal of Organic Chemistry* 82, no. 17 (2017): 9047–9053, https://doi.org/10.1021/acs.joc.7b01515.

66. S. Peng, L. Wang, J. Huang, S. Sun, H. Guo, and J. Wang, "Palladium-Catalyzed Oxidative Annulation via C–H/N–H Functionalization: Access to Substituted Pyrroles," *Advanced Synthesis & Catalysis* 355 (2013): 2550, https://doi.org/10.1002/adsc.201300512.

67. L. Jiadi, L. Bingling, H. Peisen, et al., "Meta-, Regioselective Amination of Cyclic Diaryliodoniums through C–I and C–O Bond Cleavages: an Access to Functionalized Coumarins," *Journal of Organic Chemistry* 90, no. 9 (2025): 3128–3139, https://doi.org/10.1021/acs.joc.4c02094.

68. M. D. Hanwell, D. E. Curtis, D. C. Lonie, T. Vandermeersch, E. Zurek, and G. R. Hutchison, "Avogadro: An Advanced Semantic Chemical Editor, Visualization, and Analysis Platform," *Journal of Cheminformatics* 4 (2012): 17, https://doi.org/10.1186/1758-2946-4-17.

69. G. M. Morris, R. Huey, W. Lindstrom, et al., "AutoDock4 and AutoDockTools4: Automated Docking With Selective Receptor Flexibility," *Journal of computational chemistry* 30 (2009): 2785–2791, https://doi.org/10.1002/jcc.21256.

70. E. F. Pettersen, T. D. Goddard, C. C. Huang, et al., "UCSF Chimera—A Visualization System for Exploratory Research and Analysis," *Journal of Computational Chemistry* 25 (2004): 1605–1612, https://doi.org/10.1002/jcc.20084.

71. O. Trott and A. J. Olson, "AutoDock Vina: Improving the Speed and Accuracy of Docking With a New Scoring Function, Efficient Optimization, and Multithreading," *Journal of Computational Chemistry* 31 (2010): 455–461, https://doi.org/10.1002/jcc.21334.

72. D. E. Pires, T. L. Blundell, and D. B. Ascher, "pkCSM: Predicting Small-Molecule Pharmacokinetic and Toxicity Properties Using Graph-Based Signatures," *Journal of Medicinal Chemistry* 58 (2015): 4066–4072, https://doi.org/10.1021/acs.jmedchem.5b00104.

Supporting Information

Additional supporting information can be found online in the Supporting Information section.

The Supporting Information is available free of charge. Experimental procedures, optimization details and analytical data for characterization of compounds: ^{1}H NMR and ^{13}C NMR Spectra, IR spectra, and HRMS Spectra, along with molecular docking data.

Supporting File 1: slct73258-sup-0001-SuppMat.pdf.

Supporting File 2: slct73258-sup-0002-Data.xlsx.